

SIGNAL DESIGN AND PROCESSING TECHNIQUES
FOR WSR-88D AMBIGUITY RESOLUTION
Part-6: Further Investigations

1. Introduction

The Radar Operations Center (ROC) of the National Weather Service (NWS) has funded the National Severe Storms Laboratory (NSSL) to address the mitigation of range and velocity ambiguities in the WSR-88D. This is the sixth report in the series that deals with range-velocity ambiguity resolution in the WSR-88D. The first two reports mainly dealt with the uniform PRT transmission and phase coding techniques to resolve the range-velocity ambiguity. Although the phase coding techniques do not directly address the velocity ambiguity problem, their capability to separate overlaid echoes allows the use of shorter PRTs which, in turn, diminishes the occurrence of ambiguous velocities. In report-2 investigations on all major aspects of the SZ phase coding technique is reported. It includes the practical aspects such as window effect, receiver noise, ground clutter filtering etc. The effects of the random as well as the systematic phase errors in the radar system are also investigated in order to arrive at the practical limits of performance of the phase coding scheme. The decoding when the overlay is from any two of the first four trips was explained, and multiple trip overlay situation is also presented in some detail.

Subsequent to the development of the SZ phase coding technique, C.Frush, (1999) came up with the “substitution method” for the reconstruction of the weaker signal spectrum after the notch filtering. Although the exact details of the method used by C.Frush were not available at the time of writing the report-5, we used the philosophy of substitution method and implemented it in our own way into the Matlab simulation program. A comparison of the performance of the SZ-1 algorithm using the magnitude deconvolution, and the SZ-1 algorithm using this substitution method is made on simulated time series data. The results of this comparison are given in report-5, section-2.

Siggia and Passarelli, (2002) developed their own version of the substitution method and implemented it on the Sigmet RVP7 processor. The details of the method were provided to us in the Sigmet internal notes (Siggia and Passarelli, 2002). We have coded this algorithm and compared the performance of the method with the SZ-1 algorithm described in report-2. This comparative study is presented in section 2 of this report.

While the SZ phase coding scheme is shown to be effective in resolving two overlaid echoes for overlay power ratios as large as 40 dB (with random phase error included), the presence of ground clutter posed some problems. If the clutter is to be filtered, and the 1st trip is weaker, the 1st trip spectral moments are not easily recoverable. Even though this was observed during the course of the investigations, not much time could be spent on this particular aspect. Richard Passarelli informed us that in such cases Sigmet reverts to processing as in the case of random phase code. In this report we look at this problem in more detail and present modifications in the SZ algorithm which could alleviate this difficulty to some extent. Section-3 of this report studies recovery of the spectral moments of the weak 1st trip echo in the presence of a strong 2nd trip echo and strong ground clutter.

2. Comparison of SZ-1 and Siggia's substitution algorithm

A demonstration of the SZ coding and processing for mitigation of range velocity ambiguities had been made on one data set collected with the KOUN radar in 1997 (Frush et al. 2002). Evaluation of the code performance and comparison on that data set with simulation results is on going. Since then some data have been obtained with the S-Pol radar in Florida, but at the time the phase shifter on that radar had larger noise than the one on the WSR-88D. To augment our data base and verify performance in real time, ROC installed the phase shifting capability on the KOUN radar and obtained software from Sigmet to generate and process SZ coded data. We thus planned to evaluate the performance of the code. This was to be done in two ways. One, by observing the display on the Sigmet Iris system; and two, by recording time series data and processing the signals. As of this writing we are at the beginning stage of this process. Moreover, we are developing the capability to control the phase shifter on the Research and Development WSR-88D Research Radar Data Acquisition (RRDA) system. Shortly we anticipate data collection through either platform.

Meanwhile we have obtained a report from Sigmet that describes their implementation of the

SZ processing. Sigmet had adapted their processing of random phase coded signals to the processing of the SZ coded data. This is expedient and adequate to test the code, but is not equivalent to the processing algorithms SZ-1 and SZ-2 that we have extensively analyzed. In the random phase code method of processing Sigmet notches a part of the spectrum containing the strong signal and replaces it with noise-like spectral components. Thus a natural and easy way to quickly implement the decoding for Sigmet was by using a version of the substitution method. In it they have a way (Siggia and Passarelli, 2002) to determine the correct phase of spectral replicas that differs from what Sachidananda (2001) suggested and demonstrated in simulations. This could cause some difference, but the more important difference is in estimation of the velocity. Previous simulations indicate that the best statistical performance is obtained if the mean velocity is obtained from the two spectral replicas. That is, the weak signal is re-cohered by inverting the truncated spectrum, adjusting the phases of the time series and computing autocovariance at lag one. Because Sigmet's processing differs in this important detail we decided to simulate it and compare with the proposed scheme of Sachidananda (1998).

The performance of the SZ-1 algorithm (report-2) and the substitution method of Siggia are compared with respect to the standard error in the velocity and width estimates using these two algorithms. The SZ(8/64) phase coded time series is simulated using different overlay power ratios from 0 to 70 dB, and the weaker signal velocity is estimated using the two algorithms. The errors are computed as the difference between the estimated parameters and the corresponding values input to the time series simulation program. The velocity difference between the two trip signals is varied over $\pm 28 \text{ m s}^{-1}$ velocity interval. The extreme ends are avoided to exclude velocity folding appearing as estimation error.

2.1 SZ-1 algorithm

The SZ-1 algorithm is explained in report-2 (Sachidananda et.al. 1998). To estimate the parameters of the weaker signal, the stronger signal is cohered and $3/4^{\text{th}}$ of the spectrum centered on the mean velocity of the stronger signal is notched out. The remaining $1/4^{\text{th}}$ of the spectrum is re-cohered for the weaker signal. This re-cohered signal spectrum has side bands which do not bias velocity, or increase the standard error in the velocity estimate. However, the spectrum width is biased by the side bands. To estimate the width a magnitude deconvolution is applied to the

spectrum; this shifts most of the sideband power to the original location. The spectrum width is estimated from this deconvolved spectrum.

2.2 Siggia's substitution algorithm

We based our simulation on the description given by SIGMET in their internal note: SZ(8/64) and other phase codes, April 2002. The pertinent text extracted from that note follows.

The RVP7's real-world implementation of the SZ(8/64) algorithm builds on the theory from the previous sections, but in a way that provides a robust velocity estimator having a graceful failure mode. The following procedure describes second-trip signal recovery from range bins that are coherent with the first-trip; but the exact same algorithm is run a second time to extract cleaned first-trip data.

1. We begin by computing the cross correlation sums from the inner portion of the above formula for Key . This is done for all pairs of octants that are spaced either one, three, five, or seven apart. It turns out that the code's phase difference uniqueness property between adjacent octants actually generalizes to any pair of octants that are an odd number of octants apart. This is very important because it gives us a much larger set of pairs to choose from.
2. In addition to all of the pairings from #1, we further compute the exact same set of cross correlation sums but with the octant boundaries circularly rotated by one sixteenth of a revolution (half an octant). This is to deal with anomalies that could otherwise result when the coherent power is awkwardly split by an octant seam. Note: the total number of trial pairs that result from #1 and #2 is 32.
3. Given all the cross correlation terms from #1 and #2 we then find which pair of octants (call them "left" and "right") optimize the following figures of merit (applied in the order listed).
 - The individual powers in the left and right octants are within F -dB of each other. That is a "flatness" criterion that we expect to be met by any two octants that are free of coherent power, i.e., consist only of spectral replicas and noise, both of which are flat across all octants.

- The combined left and right power is not more than P -dB stronger than the corresponding sum from any other pair of octants. This is a “cleanliness” criterion that rejects octants that clearly contain coherent power.
 - The “SQI” of the octant pair (ratio of cross correlation magnitude to total power) is maximized. This is a signal quality criterion that preferentially finds the octant pair that will produce most reliable *Key*.
4. If #3 produced a pair of octants having a suitable high SQI, then the algorithm proceeds by discarding the other six octants and replacing them with phase adjusted spectral replicas. The left octant is copied three times to its “left”, using the octant pair’s original 1,3,5, or 7 spacing, and applying the code’s phase correction at each copy. Likewise, the right octant is copied three times to its right. We now have a “whitened” power spectrum of properly phased second-trip replicas for which all first-trip coherent power has been removed.
 5. If #3 failed to produce any octants having a suitable SQI, then chaos would certainly result from step#4 because the value of *Key* could not be trusted. In this case, the RVP7 simply reverts to its normal spectral whitening algorithm. Our simulations with synthetic targets have shown that the standard random phase whitening technique are successful often enough to be worth giving them a try in these cases.

2.3 Results

Simulations were carried out with overlay power ratio, p_1/p_2 , from 0 dB to 70 dB, at 2dB intervals (i.e., the first trip echo is made stronger), and the second trip velocity and spectrum width are estimated using the two algorithms. The spectrum width of the first trip is kept fixed at 4 m s^{-1} , and spectrum width of the second trip is varied between 2 m s^{-1} and 8 m s^{-1} , in steps of 2 m s^{-1} . The velocity difference between the two trips is varied between -28 m s^{-1} and $+28 \text{ m s}^{-1}$. The last 4 m s^{-1} in the unambiguous interval of 32 m s^{-1} is left out to avoid aliased velocities appearing as estimation error.

Fig. 2.1 is a sample scatter plot of the error in the estimated velocity as a function of the overlay power ratio, p_1/p_2 . The velocity of the second trip echo is estimated using the substitution

algorithm of Siggia. The mean and standard deviation of the error is also shown in the figure. The parameters used in the simulation are indicated in the figure. In this simulation both first and second trip spectrum widths are set to 4 m s^{-1} . The mean velocity seems to have a small bias of -2 m s^{-1} and the standard error is fairly high, around 3 to 4 m s^{-1} . The high standard error is perhaps because of the way in which the spectrum is cut into 16 pieces in the substitution method. This is too coarse a discretization of the spectrum. A corresponding result for the SZ-1 algorithm is in Fig. 2.2. All the parameters of the simulation are the same except the algorithm used for estimation is the SZ-1 algorithm. The standard error in the velocity estimate is clearly under 2 m s^{-1} , and there is no bias in the estimate. The von Hann window is used in both cases, although Siggia's write-up does not mention the window. Without the window the standard errors would be much higher. Fig. 2.3 shows a comparison of the overall performance of the two algorithms with respect to the standard error in the velocity estimates for different spectrum widths. Clearly the SZ-1 algorithm performs much better than the version of the substitution method implemented by Siggia and Passarelli.

In Figs. 2.4 and 2.5 are the scatter plots of the spectrum width errors using the substitution and the deconvolution algorithms. Here again, the simulated spectrum width is 4 m s^{-1} , for both 1st and 2nd trip echoes. Whereas the deconvolution method performs reasonably well in recovering the spectrum width of the weaker echo up to an overlay ratio of 60 dB, the substitution algorithm consistently underestimates the width by about 2 m s^{-1} . Although the standard error of the substitution method is smaller, it is computed with respect to the biased mean and hence is not a fair metric for comparison. The bias is due to the truncation of the spectrum to $1/8^{\text{th}}$ of the number of coefficients and it is not a function of the true spectrum width which is not known.

An overall performance comparison with respect to width estimation is given in Fig. 2.6. It is clear that the lower standard error in the width estimates for larger widths is because of the truncation mentioned earlier. Fig. 2.7 shows the bias error in the estimated spectrum width using the substitution and the deconvolution methods. It is clear from this figure that the substitution method produces highly biased width estimates. The substitution works for very narrow widths ($<2 \text{ m s}^{-1}$) only.

2.4 Conclusions

In this section a comparison of performance of the substitution method of Siggia and

Passarelli (2002) is made using simulation. The weather signal time series is simulated with appropriate spectral parameters and SZ phase coding, and the time series is processed through the two algorithms. The resulting spectral estimates are compared with the actual input parameters to the simulation program to extract the estimation error. A large number of simulations were carried out to generate the error statistics.

The results indicate that the substitution method works only for signals having widths less than 2 m s^{-1} . Exact reconstruction is possible only if the “narrow” spectra criterion is satisfied exactly. The SZ-1 algorithm on the other hand works for much larger widths. The SZ-1 algorithm tolerates overlap of the spectral replicas, hence works for widths as large as 6 m s^{-1} .

For estimating mean velocity neither deconvolution nor substitution is needed. Direct inversion of truncated spectra, recohoring, and pulse pair processing, as described in Sachidananda et al. (1998), produces best estimates.

Substitution or deconvolution is needed for estimating spectrum width. The current version expediently implemented by Sigmet is clearly not a choice for the WSR-88D. The more complex version of substitution method suggested by Sachidananda et al. (2001) is preferred. Nonetheless, the cited reference indicates that deconvolution has a marginally better performance. Furthermore, for real time implementation deconvolution might have an advantage because it involves a simple matrix multiplication and avoids searching (an awkward operation with large overhead on real time signal processors) for the correct position of the spectral replicas.

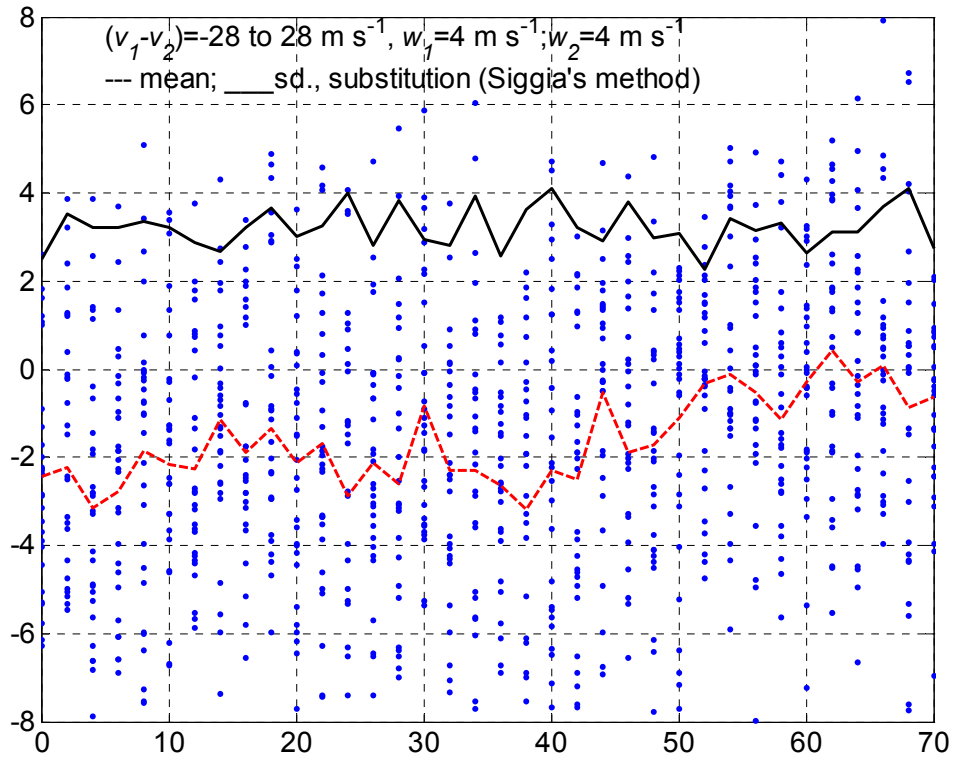


Fig. 2.1 The scatter plot of error in the velocity estimate using Siggia's substitution method.

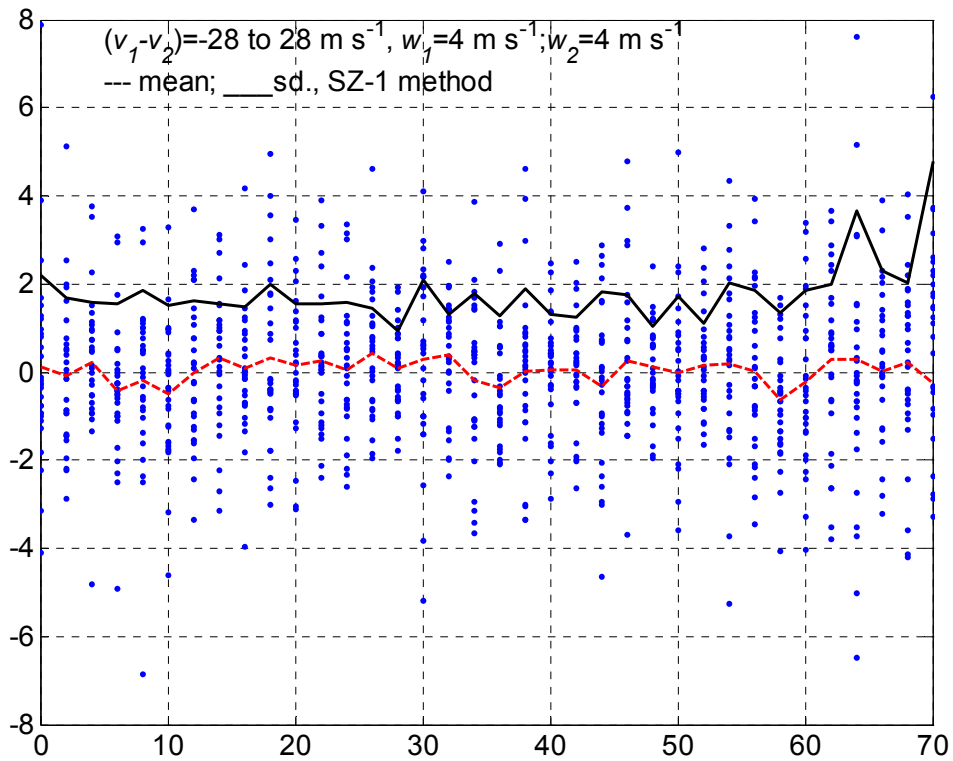


Fig. 2.2 The scatter plot of error in the velocity estimate using SZ-1 algorithm.

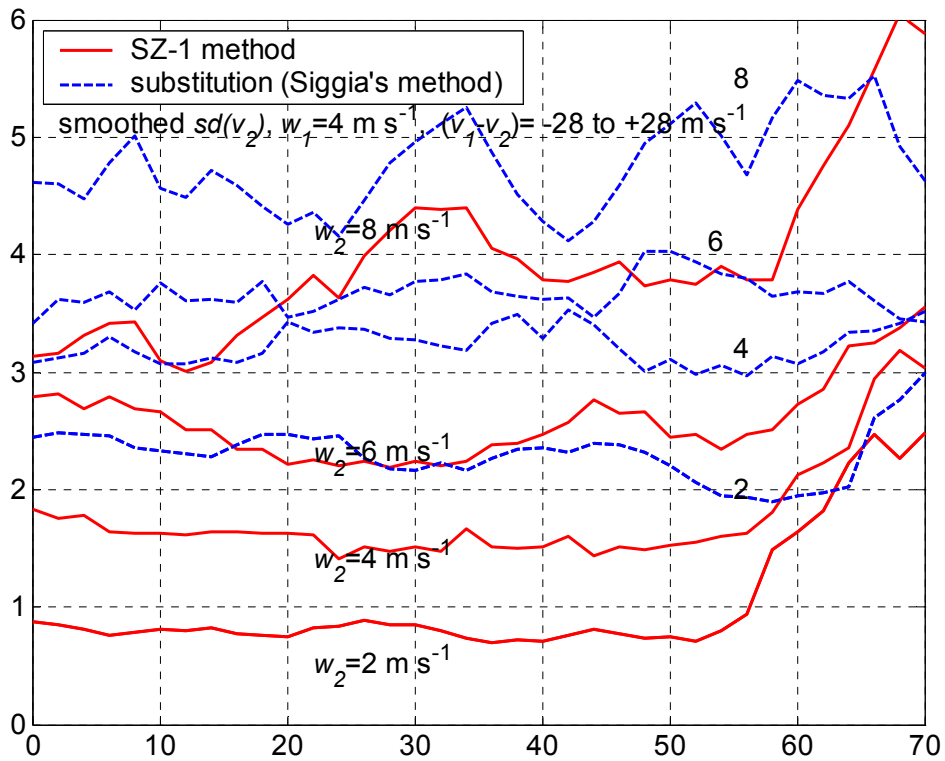


Fig. 2.3 A comparison of the standard deviation in the velocity estimate using the substitution and the SZ-1 algorithms.

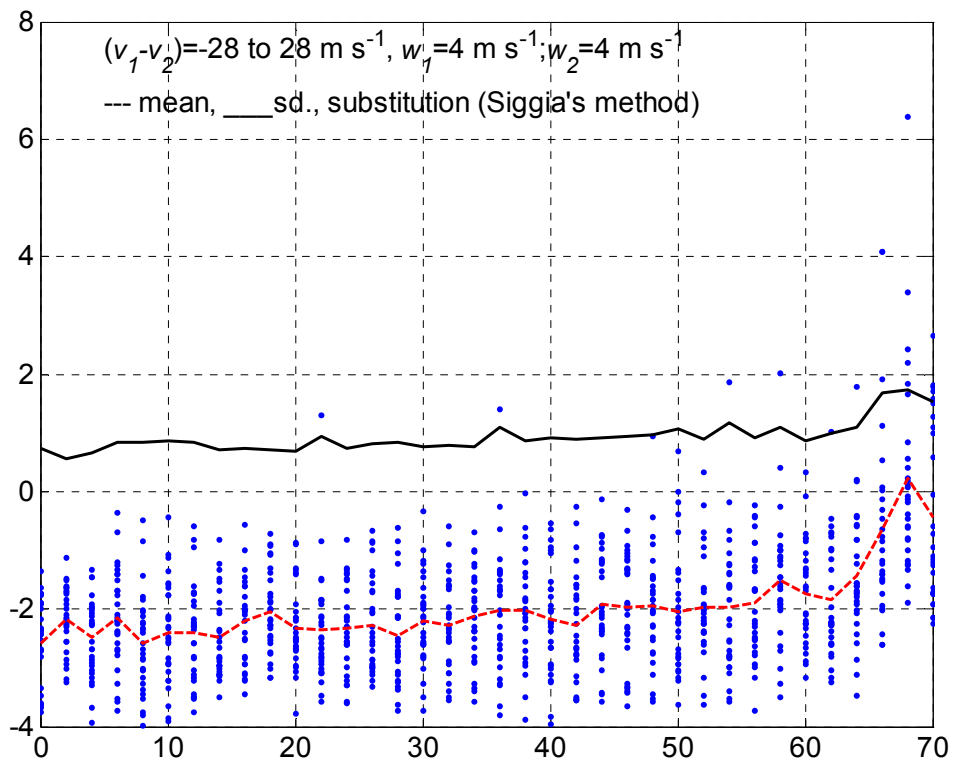


Fig. 2.4 The scatter plot of error in the spectrum width estimate using Siggia's substitution algorithm.

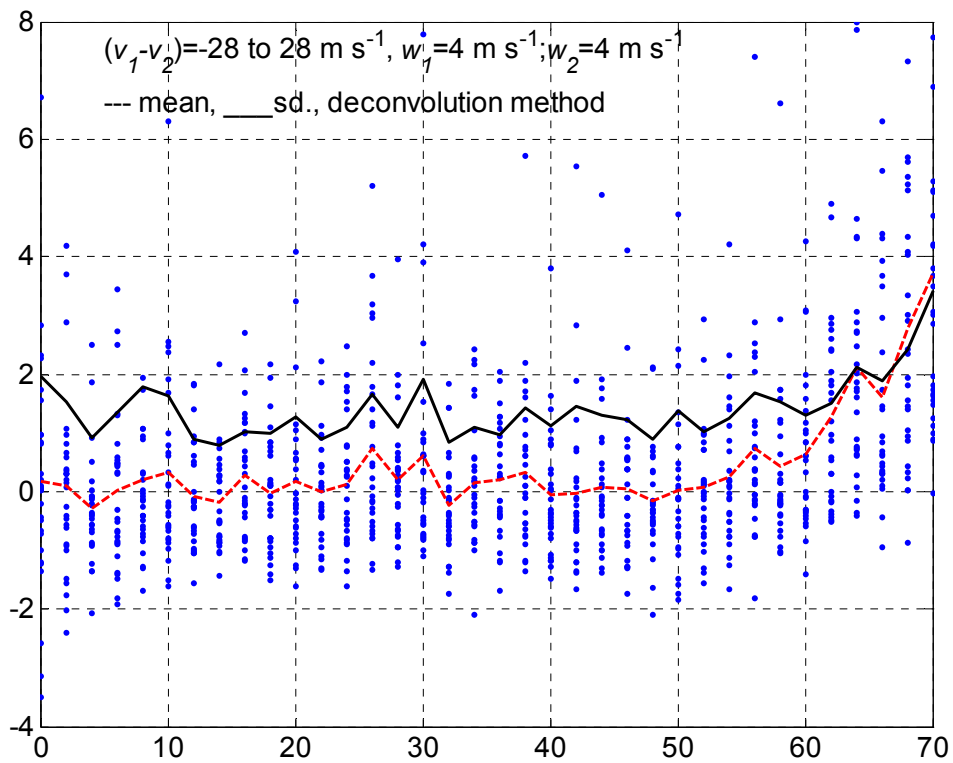


Fig. 2.5 The scatter plot of error in the spectrum width estimate using the deconvolution algorithm.

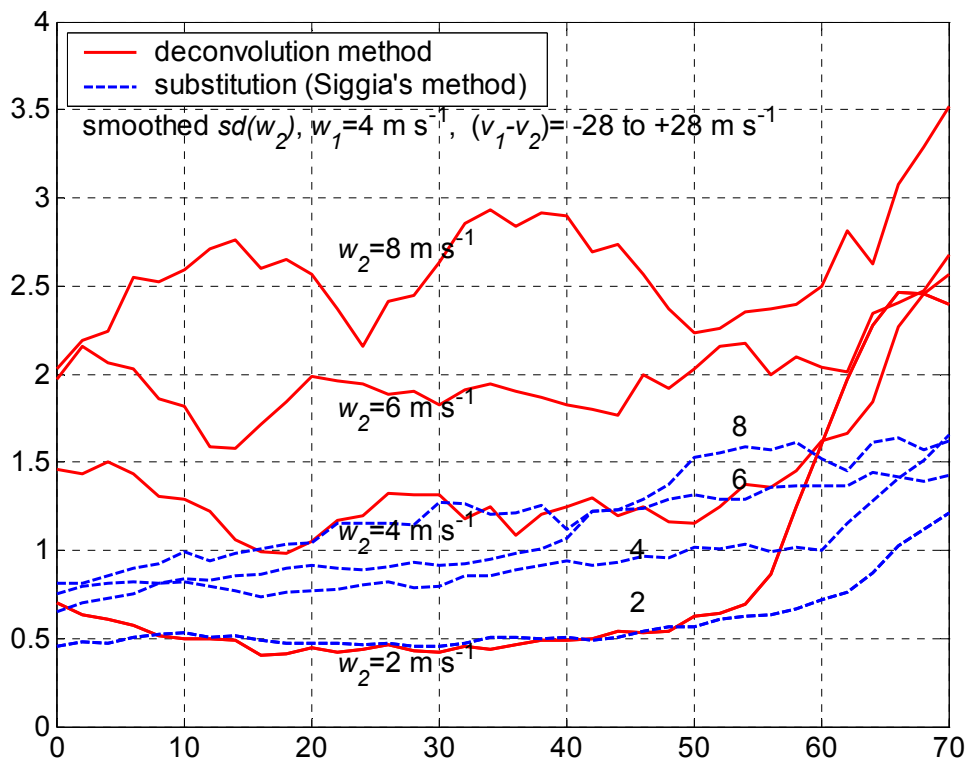


Fig. 2.6 A comparison of the standard deviation in spectrum width estimates using the substitution and deconvolution methods.

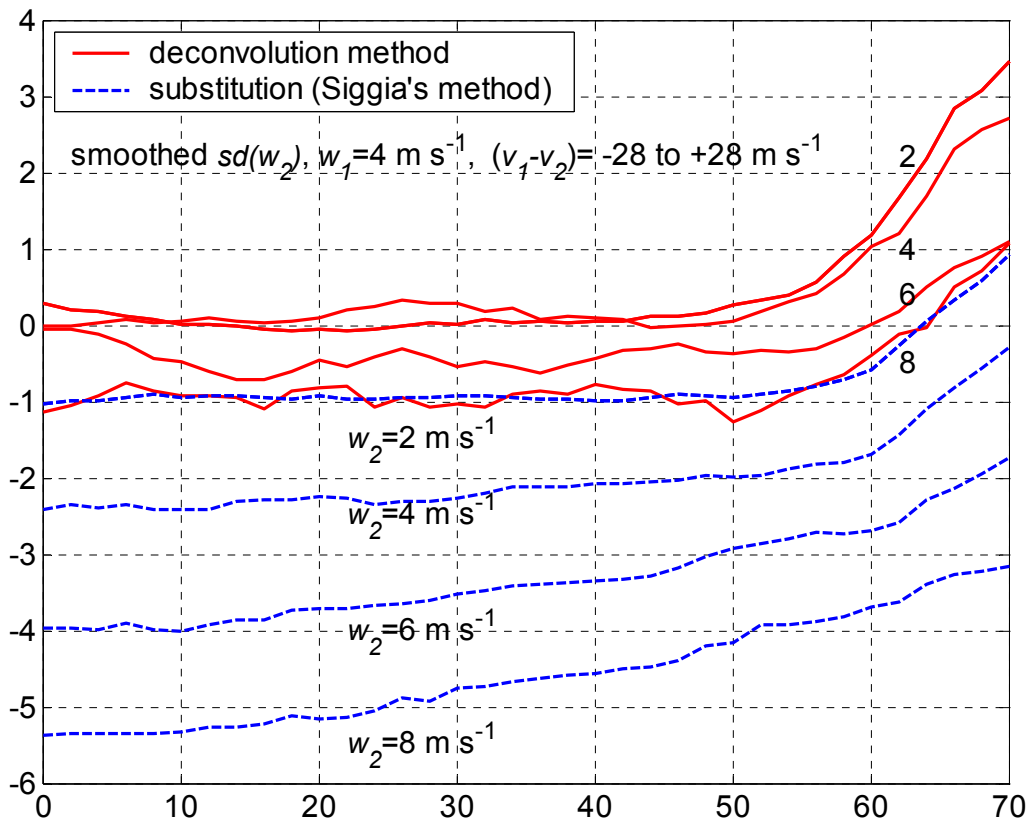


Fig. 2.7 A comparison of the bias error in the spectrum width estimate using the substitution and the deconvolution methods.

3. Ground clutter filtering in SZ phase coded radar

3.1 Introduction

Ground clutter filtering in the context of processing the SZ phase coded radar has been discussed in some detail in report-2 (Sachidananda et al. 1998). Specific procedures for processing the overlaid echoes from the 1st and 2nd trips along with ground clutter are available in that report. Furthermore, the information provided in that report is sufficient to develop the computer code. It is indicated that in the presence of the ground clutter there exists an optimum clutter filter width as well as an optimum position for the notch filter to recover the weaker signal spectral parameters. In all the cases discussed it was assumed that the 1st trip echo is stronger, and we have tried to estimate the parameters of the weaker 2nd trip echo. In the absence of the clutter filtering, the processing sequence does not depend on the trip number; we start with cohering the stronger echo. However, if the ground clutter filter is included, the sequence of processing steps is different, and depends on whether 1st trip or the 2nd trip echo is stronger. The case with 1st trip stronger is simpler, and is discussed in some detail in report-2. If the 2nd trip is stronger and strong clutter is present, the recovery of the weaker 1st trip parameters is more difficult. It is this case that we elaborate herein and outline a methodology for the implementation of clutter filtering.

Because we are using a uniform PRT, the ground clutter can be easily filtered with a notch filter of appropriate width centered on the zero Doppler. The ground clutter filter can be implemented in the time domain or in the frequency domain. Here, we have chosen frequency domain filtering because the spectral processing is already a part of the algorithm. There are two filters involved in the SZ-1 processing algorithm, one is the ground clutter filter (GCF), and the other a process notch filter (PNF) needed to recover the weaker signal parameters. Although, more than two trip echoes can be present in the actual time series obtained from a radar, here we shall consider the case of only first two trip overlay. The procedure can be extended to cases of overlaid echoes from any two of the first four trips. Some modifications are nonetheless required in the SZ-1 algorithm, because the modulation codes are different for different trips. To cohere any given trip, an appropriate phase code sequence has to be used. The rest of the procedure remains more or less the same.

The ground clutter spectrum is generally very narrow and centered on zero Doppler; a typical

clutter spectrum width in WSR-88D is about 0.28 m s^{-1} . We shall use this width in most of our illustrations. The GCF is implemented by simply deleting from the spectrum the required number of spectral coefficients centered on the zero Doppler. The spectral peak of the clutter signal can be as large as 70 dB with respect to the noise floor of the receiver, and the clutter power can spread to the rest of the spectrum via the side lobes of the window function. Thus, the application of an appropriate window is mandatory first step in processing the time series. We chose the von Hann window in our algorithm. Various aspects about the selection of the window are brought out in report-2 and hence we shall use the von Hann window without any further discussion. Another assumption is that both the 1st and 2nd trip echoes have a signal-to-noise ratio (SNR) greater than 20 dB, i.e., the effect of noise is not considered.

3.2 Optimum clutter filter width

As mentioned in the previous section the clutter-to-noise ratio (CNR) has a large dynamic range and we need to select an appropriate clutter filter width. First we address the issue of optimum filtering and arrive at some quantitative results for the selection of the filter width. Conventionally one would define an optimum filter as the one that optimizes the SNR, assuming the residual clutter after filtering as the noise. This is typically a filter whose pass band is matched to the signal spectrum. However, this definition cannot be used in the present context because we do not know the signal spectrum. The signal can be anywhere in the entire Nyquist interval, only the clutter is known to be at zero Doppler. We assume that the clutter and the signal spectra are Gaussian in shape, which is described by its mean power, mean velocity and the spectrum width. Assuming that the signal is equally likely over the entire Nyquist interval, the optimum clutter filter is the one whose stop band matches that of the clutter spectrum. In fact such a filter function is given by the inverse of the clutter spectral power envelope function, inverted about the noise floor. For an M point discrete Fourier transform (DFT) the spectral coefficients of the clutter power can be expressed as

$$|s(k)|^2 = \frac{p_c}{\sigma_c \sqrt{2\pi}} \left[\exp\left\{\frac{-k^2}{2(\sigma_c M / 2v_a)^2}\right\} + \exp\left\{\frac{-(k-M)^2}{2(\sigma_c M / 2v_a)^2}\right\} + \exp\left\{\frac{-(k+M)^2}{2(\sigma_c M / 2v_a)^2}\right\} + \exp\left\{\frac{-(k-2M)^2}{2(\sigma_c M / 2v_a)^2}\right\} + \dots \right]; k = 0, 1, 2, \dots, M-1. \quad (1)$$

where p_c is the mean clutter power, σ_c is the clutter spectrum width, and v_a is the unambiguous velocity. Because of the sampling period, the spectrum gets aliased several times over. This expression (for simplicity) contains only the fundamental, once, and twice aliased components. The optimum filter function, $F(k)$, defined in the DFT domain frequency response, is obtained by inverting the spectral power envelope function about the noise power p_n .

$$F(k) = p_n / [|s(k)|^2 + p_n]; \quad k=1, 2, 3, \dots, M \quad (2)$$

The half power points of the filter transfer function are obtained by equating the spectral envelope function to the noise level.

$$\left[\frac{p_c}{\sigma_c \sqrt{2\pi}} \right] \exp\left\{\frac{-v^2}{2\sigma_c^2}\right\} = p_n \quad (3)$$

Solving for Doppler velocity v at which the clutter power is equal to the noise, we get the half width of the clutter filter as

$$\frac{w_{cf}}{2} = \left[2\sigma_c^2 \ln\left(\frac{p_c/p_n}{\sigma_c \sqrt{2\pi}}\right) \right]^{1/2} \quad (4)$$

In practice we can replace this filter by a rectangular filter function with the notch equal to the 3dB width given by (4). Simulation shows that the quality of the spectral moments recovered by employing the filter (2) is nearly the same as the quality of moments obtained with the equivalent rectangular filter. The rectangular filter is easier to implement and it avoids one set of multiplications. It suffices to just delete the n_c spectral coefficients centered at zero Doppler, where

n_c corresponds to the filter width expressed as a number of DFT coefficients.

In practice we need a clutter filter width much larger than that given by (4) because the derivation of (4) does not include spectral broadening due to the finite number of samples. The effect of spectrum broadening due to the rectangular window is significantly reduced by using von Hann window, however, the effect of finite number of samples (finite dwell time) can not be eliminated. It can be somewhat compensated by increasing the clutter filter width. Thus, the optimum clutter filter width is a function of CNR , and apparent width of ground clutter, σ_{ca} .

Fig. 3.1 shows the pulse pair estimated width versus the number of samples, with clutter spectrum width, σ_c , as a parameter. In this plot the spectrum width is calculated using the width estimator given by Doviak and Zrnic, 1993 (Eq. 6.27) with a modification that the width is set to zero whenever $\{S/|R_1|\} < 1$, as done in WSR-88D radar. This modification sets all negative width estimates that are obtained from Eq. 6.27 to zero. These widths contribute to the mean width from a large number of simulations. The mean width calculated from simulations is almost the same as the input width. However, if we eliminate these data points and take the positive estimates alone in computing the mean we get a positive bias for low widths. The spread of $S/|R_1|$ estimates at narrow spectrum widths is such that some produce values smaller than one. If that happens then the corresponding spectrum width estimates become negative. Eliminating these estimates produces a positive bias, and setting them to zero as in WSR-88D reduces the bias. All this happens if the $SD(S/|R_1|)$ estimate is larger than $MEAN(S/|R_1| - 1)$; the standard deviation depends on the number of samples. Larger the number of samples less will be the spread, and hence, negative width estimates occur for lower values of mean width. This is illustrated in Fig.3.2(a) and 3.2(b) in which the upper plot is a scattergram of width estimates using 64 samples and the lower one is with 256 samples. Both plots use Eq.6.27 of Doviak and Zrnic (1993) as indicated in the figure. For $M=64$ the negative widths occur if $w < 2 \text{ m s}^{-1}$, and for $M=256$ negative values occur if $w < 1 \text{ m s}^{-1}$.

There are two aspects of spectrum widening which are to be considered in determining the clutter filter width. In general, the spectrum width estimate is a measure of the spread of the spectral coefficients in the spectrum. However, here we are dealing with a finite set of samples of the signal, the spectrum is obtained by DFT operation, and the width is an estimate from this finite length sequence. We are also applying the clutter filter to a finite length sequence. This distinction must be remembered while determining the clutter filter width. The spectrum width estimate can be treated

as a measure of the actual spread of the spectral coefficients in a **DFT spectrum** only for mean widths more than the standard deviation of the estimates. For mean widths less than the standard deviation, we need to take the standard deviation of the width estimate as a measure of the spread of the spectral coefficients. Thus, because the clutter signal is very narrow (around 0.28 m s^{-1}), the number of samples play a role in determining the clutter filter width needed for effective filtering of the clutter power in the spectrum. For a typical number of samples in the order of 40 to 50 (as in the WSR-88D radar), we see that the standard deviation of the width estimates is about 1.3 m s^{-1} . Hence, in designing the clutter filter we have to use this apparent width, σ_{ca} , in Eq. (4), rather than the actual clutter width input to the simulation program. For clutter signal of $w < 0.5 \text{ m s}^{-1}$, the apparent width, σ_{ca} , (about the same as the standard error in the width estimate) as obtained from simulations is $\sigma_{ca} = [2.0, 1.3, 0.8, 0.6] \text{ m s}^{-1}$ for $M = [32, 64, 128, 256]$, respectively. These are the values to be used in the clutter filter function irrespective of the actual clutter spectrum width.

It is observed through simulation studies that for typical values of $v_a = 32 \text{ m s}^{-1}$, and $M = 64$, the σ_{ca} does not fall below about 1.3 m s^{-1} , for the ground clutter. The widening effect is negligible only for $\sigma_c > 1.5 \text{ m s}^{-1}$. Because the ground clutter spectrum width is generally much lower than 0.5 m s^{-1} , the clutter filter width can be assigned a value that corresponds to $\sigma_c = 1.3 \text{ m s}^{-1}$ in Eq. (4), and this filter can be treated as the optimum for practical purposes.

Fig. 3.3 shows a plot of the clutter filter width given by Eq. (4) for different *CNR* values. The clutter filter width required to effectively recover the signal can be obtained from this plot by reading values at $\sigma_c = 1.3 \text{ m s}^{-1}$.

3.3 Processing SZ phase coded time series

The processing in the SZ decoding algorithm branches off along two different paths, depending on whether the 1st trip signal is stronger or weaker than the 2nd trip signal. These two situations require separate considerations because the ground clutter is present always in the 1st trip. We denote the mean power, mean velocity, and the spectrum width of the 1st and the 2nd trips by p_1 , v_1 , w_1 , and p_2 , v_2 , w_2 , respectively. The symbol p_c is used for clutter power, and σ_c for the clutter spectrum width.

There are two points that we need to clarify regarding the SZ-1 algorithm. The first concerns the spectrum width estimates, w_1' and w_2' (step #6 of SZ-1, report-2, page-78) given by

Eq.6.27 of Doviak and Zrnic (1993). This estimator produces negative widths whenever $\{S/|R_1|\}$ is less than unity. This situation can happen for very narrow spectrum width signals such as the ground clutter. In the SZ-1 algorithm we have deleted the negative sign and used the absolute value to compute the width estimates w_1' and w_2' . The width estimate of the stronger of the two echoes is obtained using Eq. 6.32 of Doviak and Zrnic (1993) as indicated in the SZ-1 algorithm (step#6), because it provides unbiased width estimate in the presence of (phase coded) overlay from the weaker trip.

The second point that we wish to emphasize is the use of the ratio, w_1'/w_2' , in deciding whether $p_1 > p_2$ or $p_2 > p_1$ (step #7 in SZ-1 algorithm, report-2, page-78). The two width estimates, w_1' and w_2' , are obtained from the same time series sample sequence with 1st trip and 2nd trips cohered, respectively. The ratio, w_1'/w_2' , is equivalent to the ratio $\ln\{S/|R_1|\}/\ln\{S/|R_2|\}$, where R_1 and R_2 are the autocorrelations at lag T for the two sequences with 1st trip and 2nd trips cohered, respectively. Because the total power estimate, S , is the same for both the sequences, the width ratio is uniquely related to the ratio $|R_2|/|R_1|$. In our algorithm this ratio is equivalent to the ratio of spectrum widths for most spectrum widths but the narrowest ones. This is because we do not use the Eq. 6.27 as is, but delete the $sgn\{ \}$ part so that the negative tag is removed whenever it occurs (probability approaches 0.5 at very narrow widths). If this happens it might cause the equivalence to break down. In our previous simulations (reports 1 to 5) we have used large widths so that the ratios of widths or autocorrelations produce the same result. Use of $|R_2|/|R_1|$ instead of w_1'/w_2' (in line 7 of the SZ algorithms on pages 78 and 80 in report-2) simplifies computations and might be advantageous at narrow widths. Thus, we plan to examine this issue in the near future.

In SZ-2 algorithm, we do assume that the long PRT scan data is available prior to the Doppler scan, and hence we have an estimate of the overlaid powers from the 1st and 2nd trip echoes. This can be used to determine the p_1/p_2 ratio. However, we used the width ratio (steps #6 and #7 of SZ-2) for determining whether $p_1 > p_2$ or $p_2 > p_1$ because of the better performance of the algorithm for values of p_1/p_2 near 0 dB. (Note that in report-2 there is a typing mistake - the step #7 of SZ-2 algorithm should be the same as the step #7 of SZ-1 algorithm; the width estimates should have a superscript "dash" on them.) There is an increase in the standard error in the weaker echo velocity estimate near $p_1/p_2 = 0$ dB as indicated in Fig. 3.9 of report-2.

Simulation results show that if we extend the plot to the negative x-axis (for $p_1/p_2 < 0$ dB) the standard error increases drastically. Therefore, in steps #6 and #7 of the algorithm it is necessary to use the same time series samples to determine whether $p_1 > p_2$ or visa versa. A decision based on the long PRT scan data may put p_1/p_2 on the negative side of the x-axis, because of the time delay between the two scans. The p_1/p_2 ratio may not be the same for the long PRT and the Doppler scans, although they are likely to be close.

The SZ algorithm proceeds along one of the two paths depending on which of the two, the 1st trip echo or the 2nd trip echo is stronger. If there is no ground clutter, these two paths are identical except that we start with a time series in which the stronger signal is coherent. These two paths will have different effects on the spectral moment estimates of the 1st and 2nd trip signals when clutter filter is included in the processing. With an appropriate selection of the ground clutter filter (GCF) width we can effectively filter the clutter. This filtering does not pose any problem if the 1st trip echo is stronger than the 2nd. Some minor adjustment of the process notch filter position is needed under certain conditions of the stronger 1st trip velocity (see report-2).

If the 1st trip echo is stronger, the 1st trip signal parameters are obtained by autocovariance processing the time series with the 1st trip signal coherent (square law for power, pulse pair for velocity, and logarithm of pulse pair $R(1)/R(2)$ width), and the 2nd trip parameters are obtained at different stages of processing; the notch filtering, recohering, and the deconvolution steps. The effect on the parameters p_l , v_l , and w_l is similar to that in the case of an uncoded radar. The ground clutter filter (GCF) notch, centered on the zero Doppler, removes some part of the signal if v_l is small and has spectral coefficients near zero Doppler. This loss of signal underestimates the mean power (the reflectivity becomes negatively biased), and if the clutter has wide spectrum and is not completely filtered, the residual clutter power can produce a positive bias in p_l (Sirmans 1992). The mean velocity, v_l , can be biased away from the zero Doppler, if there is signal loss due to clutter filtering, or towards zero Doppler if there is residual clutter. These bias errors can be minimized by an appropriate choice of ground clutter filter notch width, w_{cf} (in m s^{-1}). The velocity bias is not a very serious problem, but the reflectivity bias due to the signal loss is important enough to require compensation or correction (Cornelius et al. 1995).

The effect of GCF on the 2nd trip signal parameter estimates depends on the mean velocity of the first trip signal, v_l . In the SZ(8/64) decoding algorithm, the signal spectrum is notch filtered to

recover the weaker signal spectrum. The filter width is $3v_a/2$ centered on the mean velocity v_l . This filter we refer to as the process notch filter (PNF). If v_l is in the interval from $(-3v_a/4 + w_{cf}/2)$ to $(3v_a/4 - w_{cf}/2)$, then the two notch filters, viz., the GCF and the PNF, completely overlap; hence, the 2nd trip parameters are affected only to the extent of clutter power spreading due to the window effect. This effect can be neglected if v_l is close to zero but can be significant if v_l is near the limit of the velocity interval specified above.

If v_l is outside the interval $(-3v_a/4 + w_{cf}/2)$ to $(3v_a/4 - w_{cf}/2)$, the GCF and the PNF notch do not overlap completely; thus, after these two filters are applied, there are not enough spectral coefficients left for the 2nd trip signal to cohere effectively (a minimum of $M/4$ coefficients are needed for cohering the weaker signal). Therefore, it is necessary to change the PNF notch width or location, or both, to retain at least $M/4$ coefficients in the spectrum. The optimum shift or change in width of PNF is given in report-2.

The situation of weak 1st trip in the presence of clutter filtering poses some problems in the recovery of the spectral parameters of the 1st trip echo. This is indicated in the report-2 but has not been analyzed or evaluated. For this particular case the procedure alluded to in that report is as follows. a) The first trip echo is cohered. b) Ground clutter is filtered. c) The 2nd trip signal is recohered. d) Spectral moments of the 2nd trip signal are computed. e) The 2nd trip signal is filtered. f) The 1st trip signal is recohered. g) Spectral moments of the 1st trip signal are computed. Next we further elaborate on this case.

If the 1st trip (and the ground clutter) echo is cohered, the 2nd trip is modulated by the SZ modulation code; hence, after the clutter filtering, the 2nd trip power is less by a factor $(1 - w_{cf}/2v_a)$. Note that this factor is derived with the assumption that the modulated spectrum has a uniform distribution of the power across the spectrum, which may not be exactly satisfied for narrow $w_2 (< 3 \text{ m s}^{-1})$. Nonetheless, the correction of p_2 estimate is satisfactory, within few tenths of a dB even for these small widths.

A more serious problem is in the recovery of velocity v_l of the weaker 1st trip echo because the stronger 2nd trip signal does not cohere fully due to the loss of the spectral coefficients around zero Doppler after GCF. That is, after cohering the 1st trip, the second trip spectrum is replicated 8 times and one or two of these replicas or a part of them is deleted by the GCF. Hence, the 2nd trip does not cohere fully because the phase modulation spreads the power in each of the spectral

coefficients to 8 spectral coefficients separated by $M/8$ coefficients; note that all 8 are needed to fully cohere the 2nd trip signal. For example if two of the 8 coefficients are deleted by the GCF, then the power that does not cohere is $1/4^{\text{th}}$ of the 2nd trip total power. Considering that this un-cohered power is spread across the spectrum (in eight octants) we expect the recovery of the weaker 1st trip velocity only if $p_1/p_2 > -3$ dB, assuming a minimum SNR of 3dB for velocity recovery (residual power is treated as noise or interference). There is a further reduction in the residual power by the PNF by a factor $3/4$ which is another 6 dB, but this notch filter deletes $3/4^{\text{th}}$ of the weaker 1st trip signal too. However, when the 1st trip is cohered, the residual 2nd trip gets spread out in 8 replicas, which does not bias the velocity but acts as noise. We therefore expect v_1 recovery for $p_1/p_2 > -9$ dB. In most cases with $M=64$ and $CNR=50$ dB, the required clutter filter will delete two out of 8 coefficients, hence the lower limit for p_1/p_2 is -9 dB. In the absence of clutter filtering this limit can be as low as -40 dB and is primarily caused by random phase errors (see Fig. 4.3 of report-2).

Fig. 3.4 illustrates the spectrum of 2nd trip echo alone at different stages of processing in the SZ algorithm; only the magnitudes are plotted against the DFT coefficient number along the x-axis. The parameters used in the simulation are shown in the figure. The DFT coefficient numbers 1 to $M/2$ correspond to the negative velocities from 0 to $-v_a$ m s⁻¹, and the coefficients from $M/2+1$ to M correspond to the positive velocities v_a to 0 m s⁻¹. For $v_a=32$ m s⁻¹ and $M=256$ used in the illustrations (Figs.3.4 to 3.7), one DFT coefficient spacing is equal to 0.25 m s⁻¹. The first plot (Fig.3.4) shows the spectrum of the 2nd trip echo alone. When the 1st trip is cohered, the 2nd trip signal is modulated by the SZ code generating 8 replicas of the original spectrum; each replica separated by $M/8$ coefficients and phase shifted (second plot). The third spectrum is after the clutter filtering; the first few and the last few coefficients are deleted by the GCF. The fourth one is after the 2nd trip is cohered. Note that it is not fully cohered and consequently has some sidebands. It is obvious that after the notch filter PNF ($n_w=3M/4$, centered on the mean velocity of the 2nd trip echo) is applied to this spectrum, side bands outside of the notch will remain. The fifth spectrum plot is after the 1st trip (non-existent in the example) is cohered. Now, the remaining side bands (within two octants of the spectrum) of the 2nd trip echo are again modulated by the SZ phase code. Thus these sidebands are spread over the entire Nyquist interval as 8 replicas, although with much smaller magnitude. Now the power in these replicas approximately equals the power that is deleted by the clutter filter and further reduced to $1/4^{\text{th}}$ or less by the PNF. This will bias the velocity of the 1st trip echo generally towards

the zero Doppler, because these residual spectral coefficients are from the location of zero Doppler. The residual 2nd trip power also produces a larger variance in the velocity estimates. Further, the spectrum width will not be recoverable; the spread of the residual 2nd trip will produce a large bias. The deconvolution will not remove these side bands because they are not from the 1st trip.

The same steps as in Fig. 3.4 are depicted in Fig. 3.5 except the 1st trip echo with a mean power 1/10th of the 2nd trip echo is added. The clutter is not introduced but the clutter filter is applied. This is done to demonstrate the effect of the residual 2nd trip signal alone on the 1st trip spectral moment estimates. The first plot in Fig. 3.5 shows the spectrum of the 1st trip coherent and the 2nd trip modulated by the SZ phase code. The overlay ratio p_1/p_2 is -10 dB. The 1st trip spectrum is centered at about the DFT coefficient #80. The rest are replicas of the 2nd trip echo. The second spectrum is after the clutter filtering; the first few and the last few coefficients where the clutter is present are deleted. The third plot is after the 2nd trip is cohered; the 1st trip is modulated. After the $3M/4$ notch filtering and cohering the 1st trip, the 1st trip spectrum is reconstructed with the side bands; this is seen in the fourth plot. The un-cohered residual 2nd trip power is also distributed throughout the spectrum. The velocity estimate from this spectrum does give the right value for v_l but with a large standard error. The last spectrum in the figure is after the magnitude deconvolution. It is obvious that the residual 2nd trip power produces several sidebands which will cause a large bias in the width estimate. In this demonstration we have deliberately chosen the widths to be narrow (1 m s^{-1}) to clearly show the effects of each step in the SZ algorithm. Broader spectra do not illustrate as well the details because of the multiple overlap of the replicas. The overlay ratio, $p_1/p_2 = -10 \text{ dB}$ is about the minimum value for which the weaker 1st trip velocity can be recovered, but with a large error that we would normally expect for $SNR = 3 \text{ dB}$. The width cannot be recovered accurately even for this overlay ratio.

To improve the performance of the SZ algorithm in this particular situation of weaker 1st trip echo ($p_1/p_2 < 0 \text{ dB}$) and a large ground clutter, we considered two alternatives. (a) Estimate the 1st trip echo velocity using only the spectral coefficients un-contaminated by the 2nd trip residuals, and (b) restore the spectral coefficients of the 2nd trip echo which are deleted by the GCF and then recohere the 2nd trip echo so that it can be filtered better. We shall discuss these two alternatives in some detail and try to obtain the condition under which these methods can be used to recover at least the velocity of the weaker 1st trip echo.

The first alternative is derived from the following observation. It is observed that the uncohered 2nd trip signal exists only in coefficients affected by the clutter filtering; i.e., if the clutter is filtered from DFT coefficient # 1, then all the coefficients separated by $M/8$ coefficients (i.e., for $M=64$, coefficients. # 1, 9, 17, 25, 33, 41, 49, 57) will have residual 2nd trip echo. Thus, if the width of the clutter filter in terms of the DFT coefficients is less than $M/8$, there will be DFT coefficient sets which will not be contaminated by the 2nd trip residuals. If we use only these uncontaminated coefficients in estimating velocity of the 1st trip, we get values fairly close but with a bias towards center of the nearest $1/8^{\text{th}}$ segment (nearest to the actual v_l) of the spectrum. This is because the GCF is centered on zero Doppler and hence the uncontaminated coefficients will always be in the middle of the $1/8^{\text{th}}$ segment. The main problem with this scheme is that most of the time the GCF width required is larger than the $M/8$ DFT coefficients; hence we will not be left with any uncontaminated coefficients. Therefore, the first alternative is not practical.

The second alternative is to restore the 2nd trip spectral coefficients lost in the process of GCF, before it is cohered and notch filtered. Two schemes were tried; (a) scheme-1 is based on the assumption that the 2nd trip echo spectrum width is “narrow” so that the spectral replicas do not overlap in the modulated spectrum, and (b) scheme-2 assumes that there is one time overlap of the replicas. We shall discuss these two schemes and present their performance based on simulation results. The first one is simpler to implement but is less effective than the second one. Obviously this is because the second scheme can work with twice the spectrum width.

(a) Scheme-1

The restoration scheme-1 is somewhat equivalent to the spectral substitution method (Frush et al. 2002; Siggia and Passarelli 2002). The main difference is that we have a major part of the spectrum available so that only a small part needs to be restored. The basic assumption is that the 2nd trip echo has a “narrow” spectrum, i.e., its spectrum has at most $M/8$ non-zero contiguous coefficients. Assuming that the 1st trip echo is weaker compared to the 2nd trip echo, we can take one set of 8 coefficients separated by $M/8$ (i.e., for example coefficients. # 1, 9, 17, 25, 33, 41, 49, 57, if $M=64$) and restore the missing one or two of these coefficients (#1 or #57, or both, depending on the filter notch width). Similarly take the next set (# 2, 10, 18, 26, 34, 42, 50, 58) and restore the filtered values; continue the process for all the $M/8$ sets of coefficients. The amplitudes in each set are the

same but the phase differences will follow a pre-determined sequence because of the SZ phase coding. The phase difference sequence is $[-22.5^\circ, -67.5^\circ, -112.5^\circ, -157.5^\circ, 157.5^\circ, 112.5^\circ, 67.5^\circ, 22.5^\circ]$ if the original spectral coefficient is in the 1st $M/8$ position. For the original spectral coefficients in other locations the sequence is cyclically rotated. The position of -22.5° is the location of the original coefficient. If the lost coefficients could be restored exactly then the 2nd trip will cohere exactly in the next step of the SZ algorithm. However, this exact coherence happens only for “narrow” spectra, and in the absence of 1st trip echo. This criterion puts a severe restriction on the spectrum width of the echo, which most echoes do not satisfy. In the absence of the ground clutter the SZ algorithm performs fairly well even if the “narrow” criterion is not satisfied (one time overlap is acceptable for SZ algorithm). But the performance of the substitution scheme-1 is not as forgiving, it requires narrow spectrum widths.

Fig. 3.6 illustrates different stages of processing in the spectrum restoration using scheme-1. Only the 2nd trip signal is present in the time series; the ground clutter and the 1st trip echo are not included to highlight the effectiveness of the spectrum restoration. We have chosen a spectrum width $w_2=2 \text{ m s}^{-1}$, which *nearly* (but not exactly) satisfies the “narrow” spectrum criterion. It has a few tail end coefficients extending beyond the $1/8^{\text{th}}$ interval. The first plot shows the phase modulated 2nd trip echo after filtering the ground clutter. The first few and the last few coefficients are deleted by the GCF. The second plot is the restored spectrum using the substitution method explained earlier. The third plot is the recohered spectrum of the 2nd trip. Note that it has been reconstructed much better than without this procedure (compare this with Fig. 3.4, 4th plot for $w_2=1 \text{ m s}^{-1}$); nonetheless, small residuals remain at a few places. These are due to the overlapping of the spectral replicas which prevent exact restoration in the substitution method. After the $3M/4$ notch filtering we are left with two of these small residual side bands, and on cohering the 1st trip echo (not present in the example) we obtain the spectrum shown in the 4th plot. The 5th one is after the magnitude deconvolution. In this example the tail ends of the 2nd trip echo spectrum are not correctly restored because of the overlap. Magnitude deconvolution (meant to restore the 1st trip) acts on these tails and produces the spectrum in 5th plot.

Next we repeat the same plots as in Fig. 3.6 but with a weak 1st trip echo ($p_1/p_2 = -10 \text{ dB}$) also included in the time series (Fig. 3.7). The parameters used in the simulation are indicated in the figure. The 1st trip signal is around the DFT coefficient # 80 ($v_1 = -20 \text{ m s}^{-1}$). It is seen that the

recovered 1st trip (plot # 4) is contaminated by the residual of the 2nd trip. The last plot demonstrates that the magnitude deconvolution does not restore the 1st trip as well as is possible without the clutter (see report-2). It has several sidebands that will severely bias the width estimate. The velocity estimate obtained from the spectrum #4 would be reasonably close to the actual but will have a large standard error.

To determine the limits for the estimation of the weaker 1st trip echo parameters, we ran simulations with a weak 1st trip echo and a large ground clutter. The spectral parameters of the weaker signal are kept constant. The parameters chosen are $SNR_1 = 20$ dB, $CNR = 70$ dB (i.e., $CSR = 50$ dB), and $w_1 = 4$ m s⁻¹. The velocity is arbitrarily chosen as $v_1 = 20$ m s⁻¹, and the unambiguous velocity, $v_a = 32$ m s⁻¹. The 2nd trip parameters are varied but with 2nd trip echo always stronger than the 1st. The errors in the spectral moment estimates of the 1st trip are computed with respect to the corresponding input parameters. The results are in the next few figures. In the figures the dots represent the error for each simulation; the mean and standard deviation of the errors are also shown. In Figs. 3.8, 3.9 and 3.10 are error plots of p_1 , v_1 , and w_1 ; the spectrum width of the stronger 2nd trip signal, $w_2 = 1$ m s⁻¹, and the spectral restoration scheme has **not** been applied after the ground clutter filter. It is obvious from these three figures that p_1 and v_1 can be recovered only for $p_2/p_1 < 5$ dB, and w_1 can be recovered for $p_2/p_1 < 0$ dB, even for $w_2 = 1$ m s⁻¹. The same simulations are run but **with** the spectral restoration scheme applied after clutter filtering and the results are shown in the next three figures (Figs. 3.11, 3.12, and 3.13). It is clearly seen that the spectral moments can be recovered for p_2/p_1 up to about 40 dB. This is a significant improvement. However, with increasing spectrum width of the stronger 2nd trip echo, the residual (due to overlap of spectral replicas) becomes significant and restoration eventually fails. The next three figures show similar plots with $w_2 = 2$ m s⁻¹ (Figs. 3.14, 3.15, and 3.16). The mean power estimate is good for $p_2/p_1 < 20$ dB and the mean velocity and the spectrum width are good only for $p_2/p_1 < 15$ dB. The estimates deteriorate very fast with increasing w_2 , which is due to the overlap of the spectral replicas in the modulated spectrum.

(b) Scheme-2

The second scheme is designed to resolve one time overlap of the spectral replicas in the SZ(8/64) phase modulated spectrum so that we can accommodate twice the spectrum width of the 2nd trip, i.e., the spread can be $2(M/8)$ coefficients. For widths larger than this the restoration is not exact.

Fig. 3.17 illustrates the original and the modulated spectrum. The modulated spectrum has 8 replicas and each replica is phase shifted with respect to the original spectrum. The phase shift sequence resulting from the SZ code modulation is $[\varphi_1, \varphi_2, \dots, \varphi_8] = [45^\circ, 22.5^\circ, -45^\circ, -157.5^\circ, 45^\circ, -157.5^\circ, -45^\circ, 22.5^\circ]$, for the original spectral coefficient in the first $M/8$. For the original coefficients in other octants, the phase shift sequence is cyclically shifted ($\varphi_1=45^\circ$ is the position of the original coefficient) The clutter filter deletes the first and the last few coefficients as shown by hatched portion (Fig. 3.17), depending on the filter width. In this illustration we have taken out $M/4$ coefficients, which is nearly the clutter filter width needed if the CNR is very large (~ 70 dB). Thus, at most we lose two replicas of the 2nd trip echo spectrum. Six replicas are left in the spectrum which can be used to restore the coefficients lost due to the clutter filter. It can be seen from the figure that any coefficient of the modulated spectrum is a sum of two of the original spectral coefficients separated by $M/8$ coefficients and multiplied by appropriate phase factors. For example, the 82nd coefficient in the modulated spectrum (Fig. 3.17, 2nd plot) is the sum of coefficient # 42 and coefficient # 62 of the original spectrum (Fig. 3.17, 1st plot), with appropriate complex multipliers. Thus, the sequence of 8 coefficients numbered 2, 22, 42, 62, 82, 102, 122, and 142, are combinations of the same two original coefficients #42 and #62 (multiplied by known but different phase factors). Of these 8, only #2 and #122 are deleted by the clutter filter, the rest are available. Thus we can write 6 equations, for the two unknowns. In fact, any two of these 6 are sufficient to solve for the two unknowns, but we shall use all six in our scheme-2 to isolate contamination by the 1st trip echo. $M/8$ such sets have to be solved to obtain all the missing coefficients.

To put this in mathematical form, let $s_o(i); i=1,2,\dots,M$, be the original spectrum (top graph in Fig. 3.17) and $s(k)$ be the spectrum after phase coding; the index i refers to the original spectrum whereas the index k refers to the spectrum after phase modulation. Let $s_o(i) = a$, and $s_o(i+M/8) = b$, be the two complex coefficients of the original spectrum (these overlap after phase coding, Fig. 3.17 bottom graph). Phase coding combines these two into the 8 coefficients, $\{s(k), s(k+M/8), s(k+2M/8), \dots, s(k+7M/8)\}, k = 1, 2, \dots, M/8$. The DFT index i is equal to one of the DFT indices in the set of 8 coefficients. In the example (Fig. 3.17), take $i = 42$, then $(k+2M/8) = 42$. Thus we can write these 8 coefficients in terms of a and b as

$$s(k) = a \exp(j \varphi_7) + b \exp(j \varphi_6), \quad (5)$$

$$s(k+M/8) = a \exp(j \varphi_8) + b \exp(j \varphi_7), \quad (6)$$

$$s(k+2M/8) = a \exp(j \varphi_1) + b \exp(j \varphi_8), \quad (7)$$

$$s(k+3M/8) = a \exp(j \varphi_2) + b \exp(j \varphi_1), \quad (8)$$

$$s(k+4M/8) = a \exp(j \varphi_3) + b \exp(j \varphi_2), \quad (9)$$

$$s(k+5M/8) = a \exp(j \varphi_4) + b \exp(j \varphi_3), \quad (10)$$

$$s(k+6M/8) = a \exp(j \varphi_5) + b \exp(j \varphi_4), \quad (11)$$

$$s(k+7M/8) = a \exp(j \varphi_6) + b \exp(j \varphi_5). \quad (12)$$

In these 8 equations the unknowns are a , and b . The phases φ_1 to φ_8 , and 6 of the coefficients on the left side are known. The clutter filter would delete at most the 1st and the last spectral coefficients, hence we are left with 6 equations, from Eq. (6) to Eq. (11). We can take any two of these 6 and solve for a and b , and then reconstruct the deleted 1st and the last coefficients using Eq. (5) and Eq. (12). For example the solution from Eq. (6) and (7) is

$$b = \{s(k+M/8) e^{-j \varphi_8} - s(k+2M/8) e^{-j \varphi_1}\} / \{e^{j(\varphi_7 - \varphi_8)} - e^{j(\varphi_8 - \varphi_1)}\}, \quad (13)$$

$$a = \{s(k+M/8) e^{-j \varphi_7} - s(k+2M/8) e^{-j \varphi_8}\} / \{e^{j(\varphi_8 - \varphi_7)} - e^{j(\varphi_1 - \varphi_8)}\}. \quad (14)$$

Similar solutions can be derived for other pairs of equations. Note that the weaker 1st trip signal is also present somewhere in the spectrum. Again assuming that the 1st trip echo spectrum also has at most $2M/8$ non-zero contiguous coefficients, two adjacent equations of the six will also contain the 1st trip echo power. But we do not know which two are affected by the 1st trip echo. Hence, we solve

all the 5 consecutive pairs of equations, (6,7), (7,8), (8,9), (9,10) and (10,11), and obtain 5 pairs of a and b values. Then we compare these values and find the two which are closest to each other as the most likely candidates to be least contaminated by the 1st trip echo. Then we use these values of a and b to determine the lost spectral coefficients, $s(k)$ and $s(k+7M/8)$. It is to be noted here that in this example we have taken a spectral coefficient on the left side of the mean velocity v . For coefficients on the right side of v , the two non-zero values a , and b , would be the coefficients $s(k)$ and $s(k-M/8)$, and hence the phase multiplier sequence for b in Eqs. (5) to (12) would be shifted back by two (i.e., $\varphi_8, \varphi_1, \varphi_2, \dots \varphi_7$).

This scheme-2 gives much better rejection of the 2nd trip echo, and recovers the weaker 1st trip spectral moments. In Figs. 3.18, 3.19 and 3.20 are plots of the errors in estimates of p_l , v_l , and w_l , respectively, for $w_2=2 \text{ m s}^{-1}$. All the simulation parameters are the same as in Figs. 3.14 to 3.16, but the processing uses scheme-2 for spectral restoration. It can be seen that there is a significant improvement in the performance of the SZ algorithm compared to the scheme-1, but the scheme-2 does need some extra computation.

The results in Figs. 3.8 to 3.20 are from simulations at specific spectrum widths. A large number of such simulations were carried out with spectrum width of the 2nd trip echo and the overlay power ratio, p_2/p_1 as parameters. The performance of the two schemes in recovering the spectral moments of the weaker 1st trip echo is summarized in Fig. 3.21. The maximum value of the overlay power ratio for which each of the spectral moments could be recovered with a reasonable accuracy is plotted as a function of the spectrum width of the 2nd trip echo. Herein reasonable accuracy means that the mean errors (bias) in p_l , v_l , and w_l are less than 1 dB, 1 m s^{-1} , and 1 m s^{-1} . The 1st trip echo spectrum width is taken as 4 m s^{-1} in all the simulations. The p_2/p_1 limits for the SZ-1 algorithm without the spectral restoration is also included for comparison. The lower limit for the p_2/p_1 is about -40 dB (see Fig. 4.3 of report-2).

If the clutter filter width is reduced (we need a narrower GCF for lower CNR) the performance is somewhat improved, but we cannot reduce the GCF width beyond a limit because of the fixed number of samples (dwell time) that we have in a practical radar. It can be seen from Fig. 3.21 that we can recover the weak 1st trip parameters only if the 2nd trip has narrow spectrum width. In general because the 2nd trip is from farther distance the width is larger, hence the upper limit of p_2/p_1 is about 15 dB, **with** the spectral restoration scheme-2. Otherwise the limit is only about 5 dB.

It is important to note that the Fig. 3.21 is for a large CNR ($=70$ dB) which requires a clutter filter width of nearly $1/4^{\text{th}}$ of the Nyquist ($n_c=15, M=64$). For a $CNR=30$ dB we need a filter width of about 9 coefficients out of 64 (see Fig. 3.3). Because the ground clutter is not always that large, in practice we can expect a slightly better performance than suggested by Fig. 3.21.

Next we mention briefly the fourth option that we tried, in which the clutter was filtered after the notch and cohere process, i.e., the stronger 2^{nd} trip echo is cohered and a $3M/4$ notch filter is applied to delete the 2^{nd} trip echo before the clutter is filtered. In this case the 2^{nd} trip echo coheres completely, hence is removed from the spectrum except for a small residual. Now, the remaining $M/4$ coefficients are cohered for the 1^{st} trip which also includes the clutter. Because of the notch filter the 1^{st} trip echo and the clutter will have side bands. This again causes the problem of overlapping clutter and the 1^{st} trip echo side bands. We can take the coefficients around zero Doppler and reconstruct the modulated clutter spectrum, and then subtract it to obtain only the 1^{st} trip echo. However this also is not exact because some side band of the 1^{st} trip echo overlaps the zero Doppler bin and hence gets deleted in the process of filtering the clutter. The remaining 1^{st} trip echo power spectrum is not the original one, but modified by the clutter filtering. This produces a highly biased estimate of the 1^{st} trip velocity. This method also did not yield good results; its performance is worse than the second method described earlier, hence is not elaborated here further.

3.4 Conclusions

In this section clutter filtering aspects in the context of SZ phase coded radar are discussed; especially the case in which the 1^{st} trip is weaker than the second trip echo. In the absence of the clutter both the trip spectral moments can be recovered for overlay power ratio in excess of ± 40 dB, but if the clutter is present and needs to be filtered, this limit is approximately $-40\text{dB} < p_2/p_1 < 5$ dB; when the 1^{st} trip echo is weaker than the second trip echo the limit is only about 5dB. Four different methods of recovering the weaker 1^{st} trip parameters have been considered. These were regular processing, scheme-1, scheme-2, and recohering and filtering the second trip first. Of the four methods scheme-2 had most promise, especially if the 2^{nd} trip echo spectrum width is less than 4 m s^{-1} .

In most practical situations the ground clutter is normally confined to the first 20 km or so, and hence the total area where the weaker 1^{st} trip velocity becomes non-recoverable is small.

Assuming a maximum range coverage with two trips to be 230 km, the fractional area where this problem can occur is $(20/230)^2 = 0.0076$ or 0.76%. If we assume equal probability to all the four possible combinations, i.e., 1st trip only, 2nd trip only, $p_2/p_1 > 0$ dB, and $p_2/p_1 < 0$ dB, the fractional area over which the 1st trip velocity is not recoverable is $0.76 \times 0.25 = 0.19$ % of the total area.

The 2nd trip parameters are not affected by ground clutter and hence can be recovered within the specified limits. Further, it is also known that the spectrum width is larger for far out range cells because of the larger volume enclosed by the antenna beam. The spectrum width is generally wider than 2 m s^{-1} , therefore even the scheme-2 will not be of much help if there is strong ground clutter and the 1st trip echo is weaker than the 2nd trip echo. It appears that the best strategy would be to have more stringent censoring criteria for recovery of the 1st trip moments in such situations than what would be normally used. Thus, more data would be ignored and recommended processing for the remaining “good data” is according to scheme-2. A recent study of the spectrum widths in different types of weather phenomena (Ming Fang and Doviak,2001), indicates that the median value of spectrum widths encountered are wide ($>4 \text{ m s}^{-1}$) only in squall lines, but in other types of storms it is in the order of 2 m s^{-1} or less. Therefore, it is expected that the scheme-2 would perform much better under such situations.

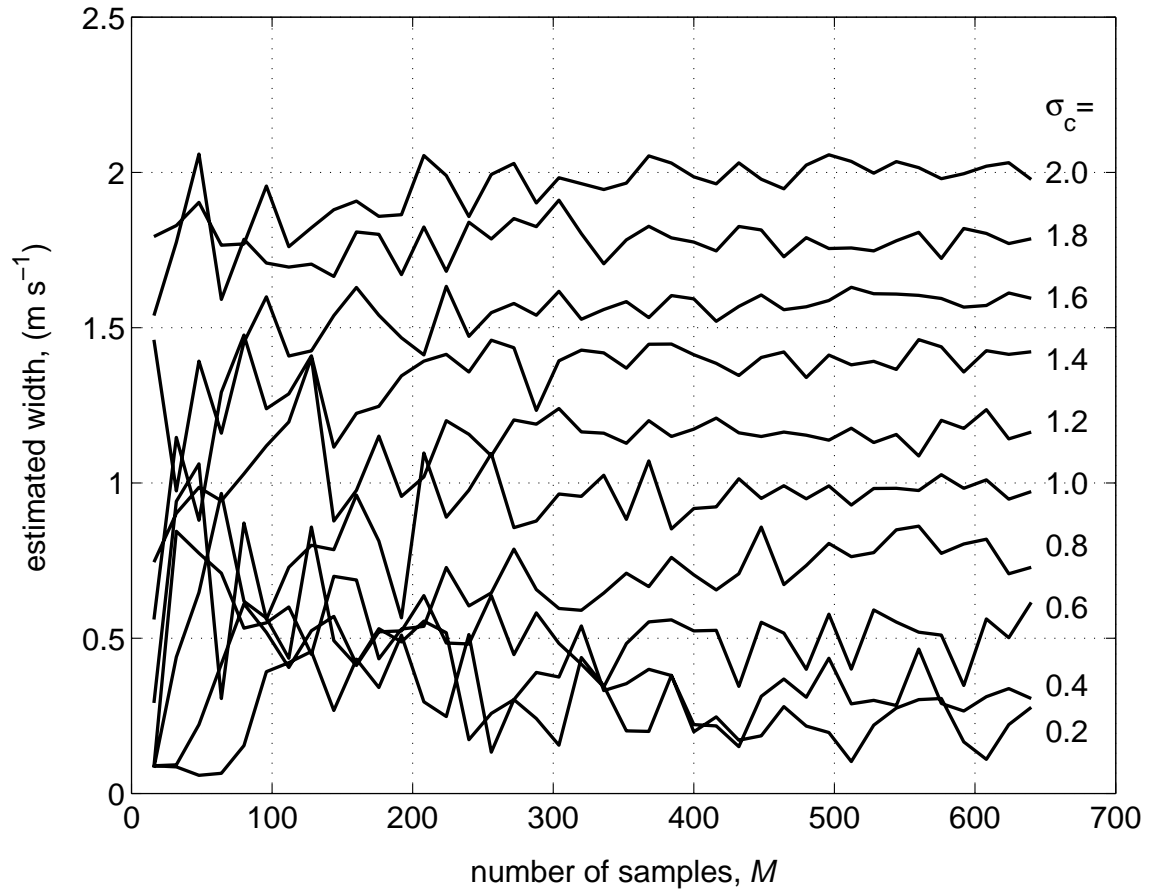


Fig. 3.1 Effect of the number of samples on the estimated clutter spectrum width.

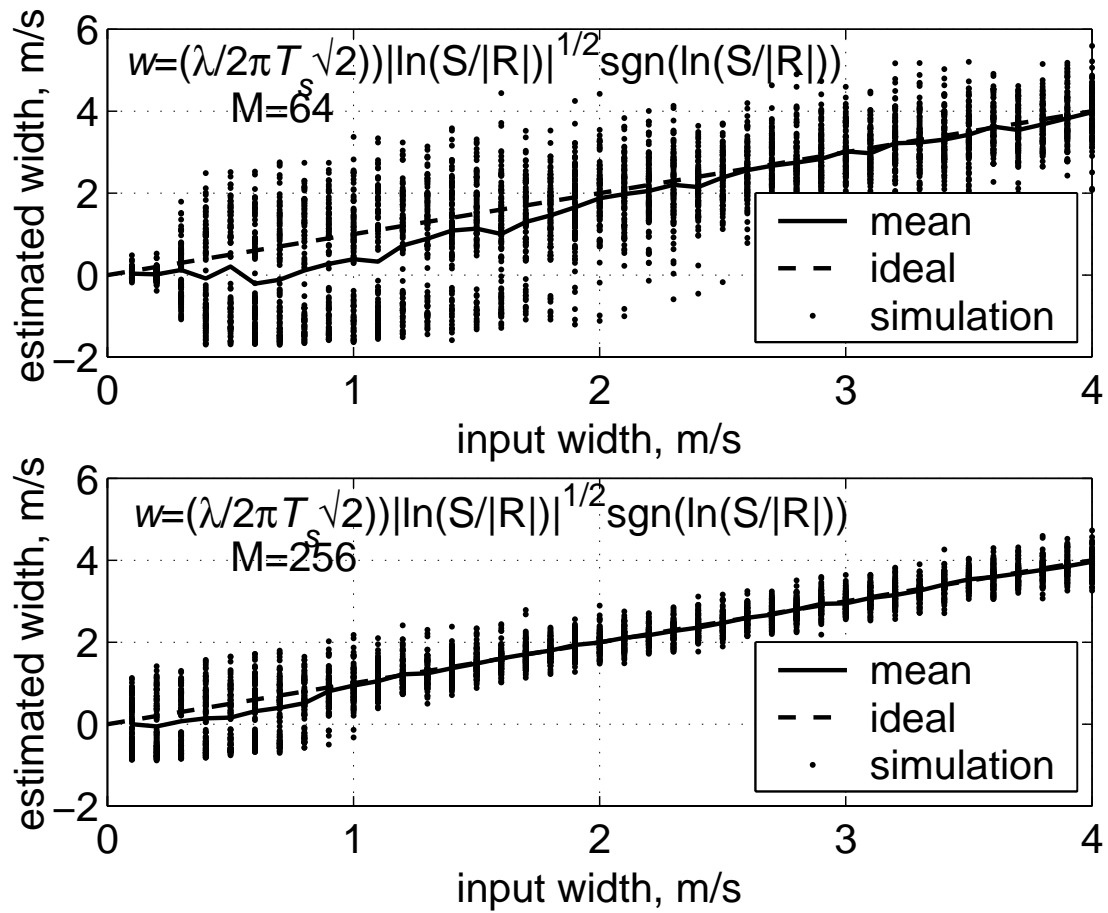


Fig. 3.2 The apparent clutter spectrum width (or the estimated width) versus the actual spectrum width for different sample sequence lengths.

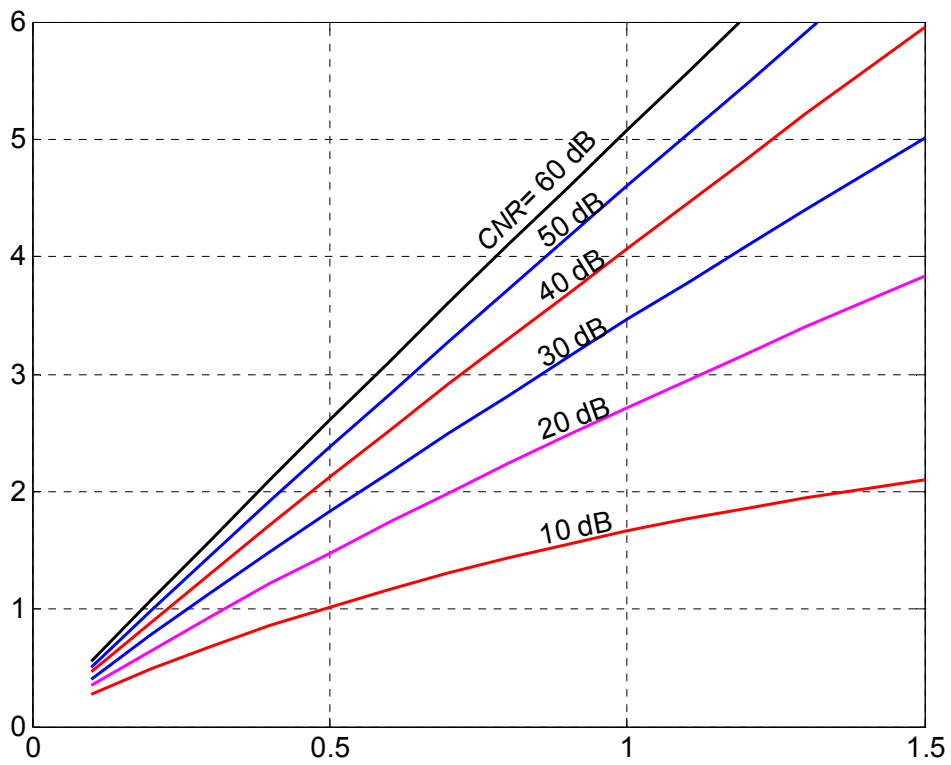


Fig.3.3 Theoretical optimum clutter filter width versus the ground clutter spectrum width.

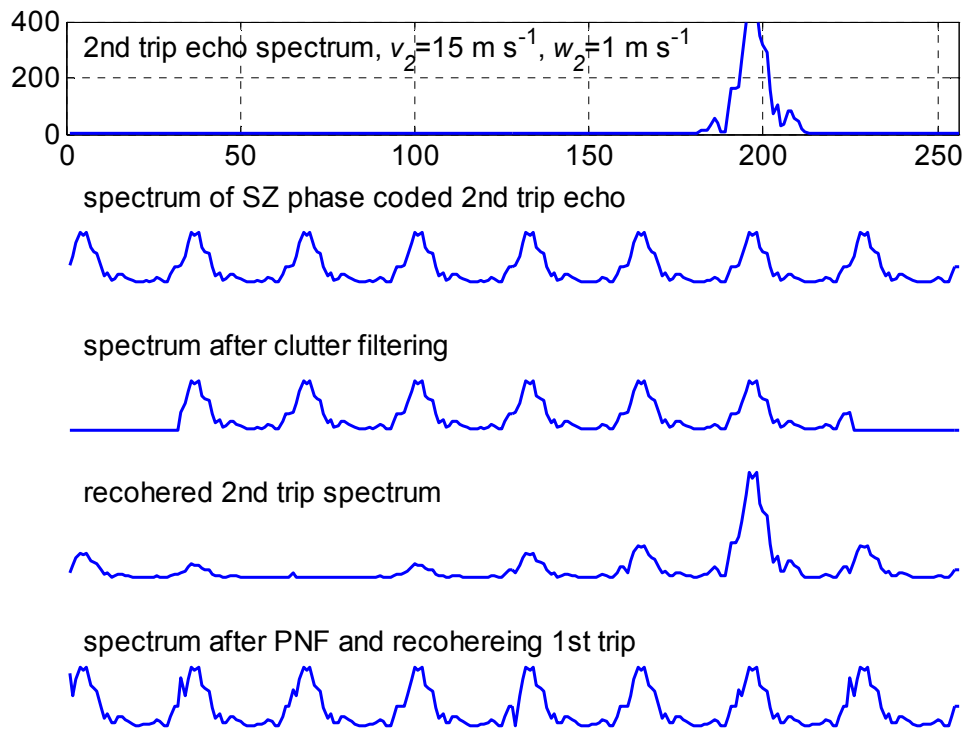


Fig.3.

4 Spectra plots of the 2nd trip echo alone at different stages of processing using the SZ algorithm.

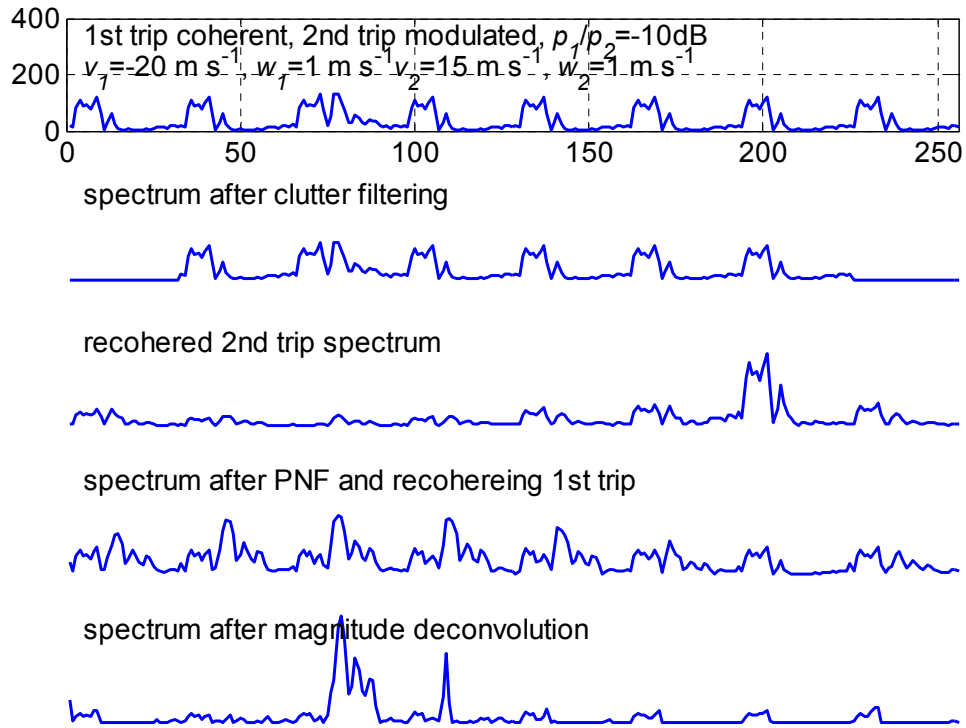


Fig.3.5 Spectra plots of the 1st and 2nd trip echoes at different stages of processing using the SZ algorithm.

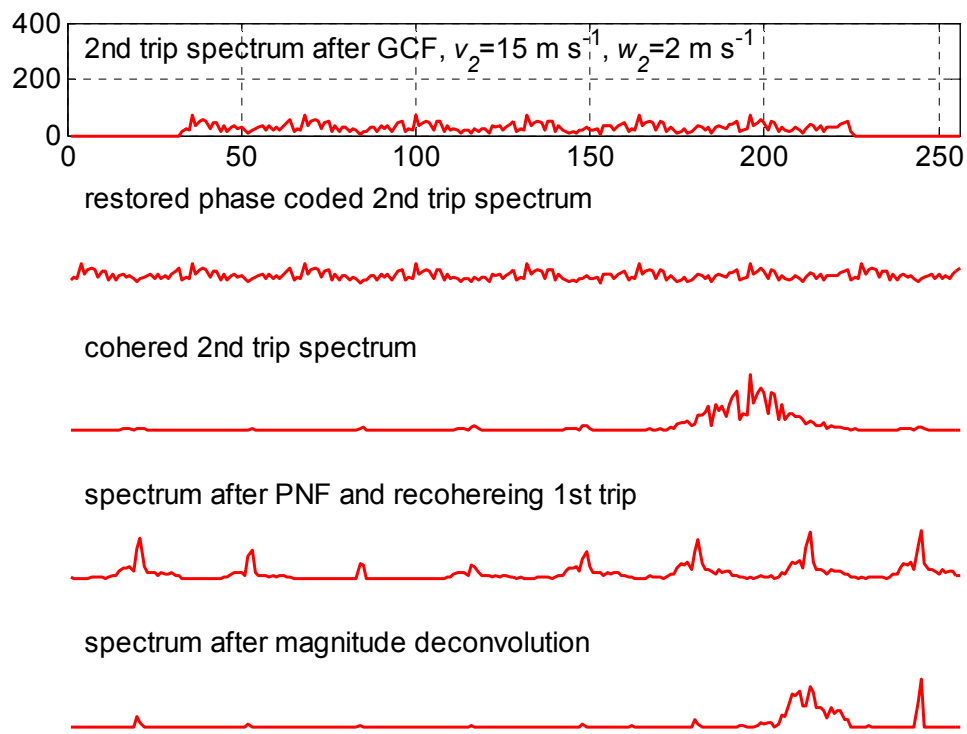


Fig. 3.6 Illustration of the 2nd trip spectrum restoration after clutter filtering.

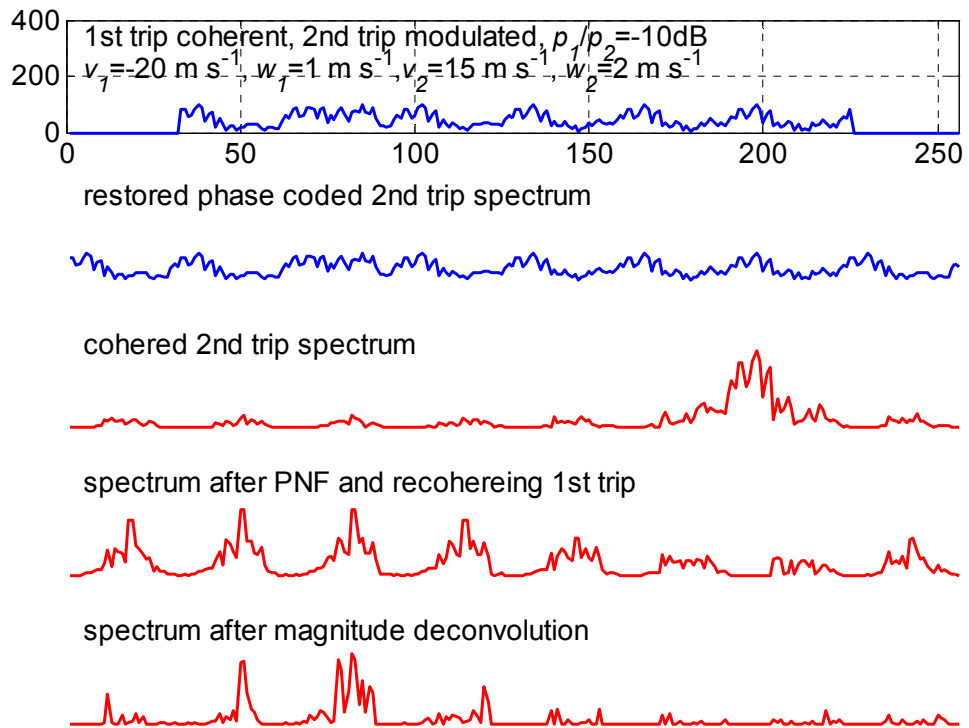


Fig. 3.7 The illustration of Fig.3.4 repeated with 1st trip signal also introduced in the time series.

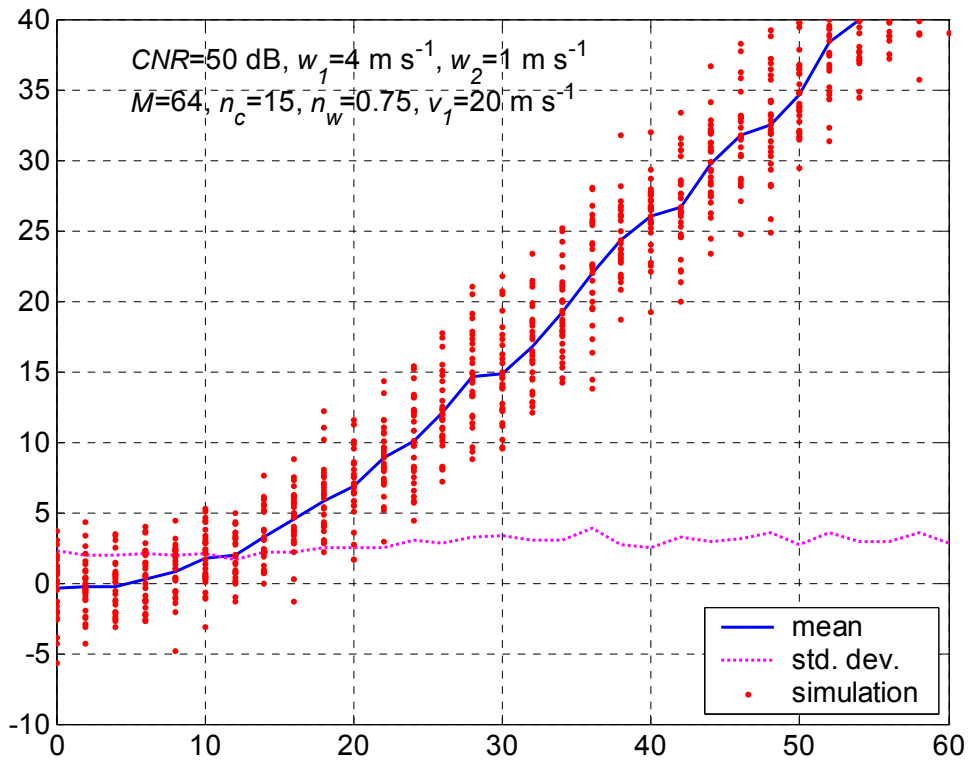


Fig. 3.8 Error in the mean power estimate, p_1 , after ground clutter filtering for $p_2/p_1 > 0 \text{ dB}$ for a $CSR = 50 \text{ dB}$ **without** the spectral restoration, $w_2=1 \text{ m s}^{-1}$.

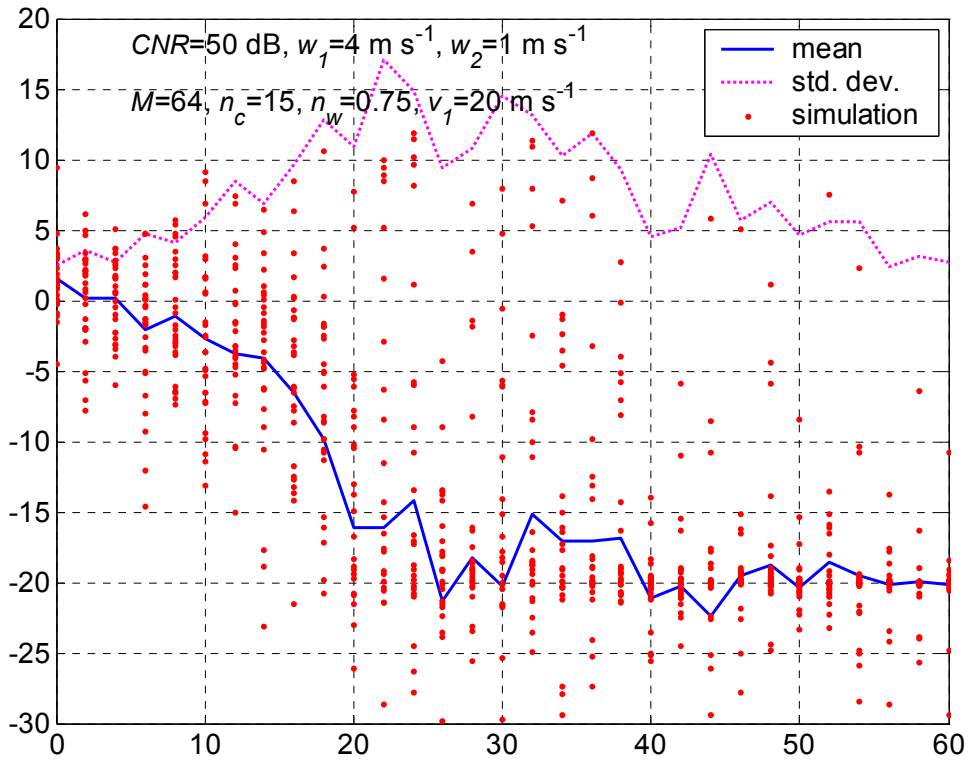


Fig. 3.9 Error in the mean velocity estimate, v_l , after ground clutter filtering for $p_2/p_1 > 0$ dB for a $CSR = 50$ dB **without** the spectral restoration, $w_2=1 \text{ m s}^{-1}$.

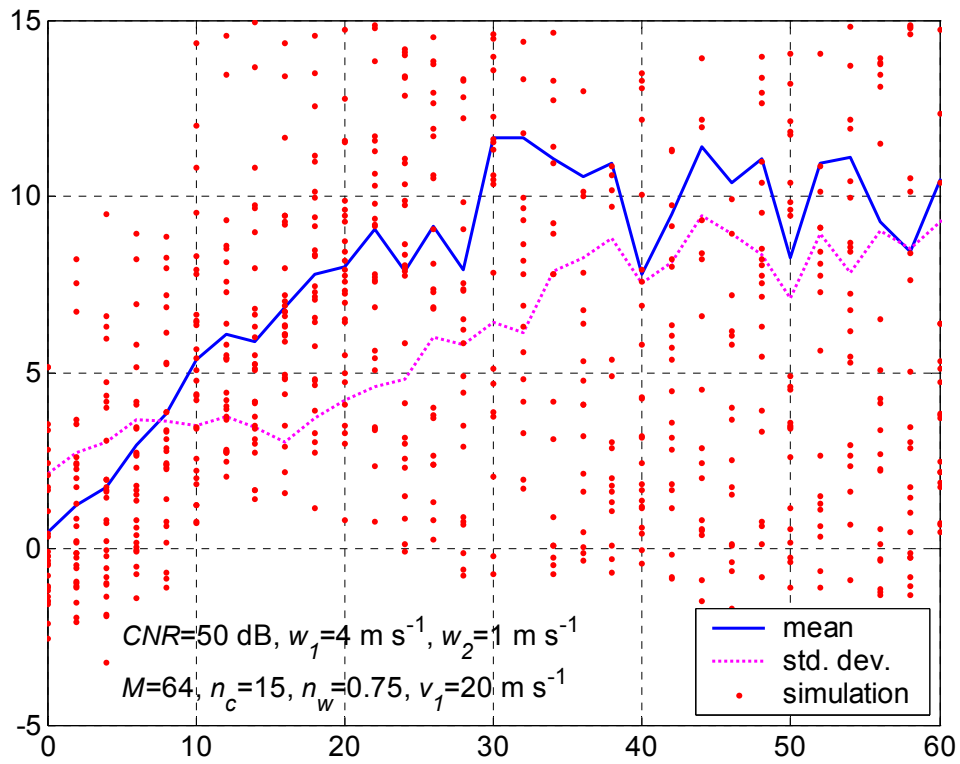


Fig.

3.10 Error in the spectrum width estimate, w_l , after ground clutter filtering for $p_2/p_1 > 0 \text{ dB}$ for a $CSR = 50 \text{ dB}$ **without** the spectral restoration, $w_2=1 \text{ m s}^{-1}$.

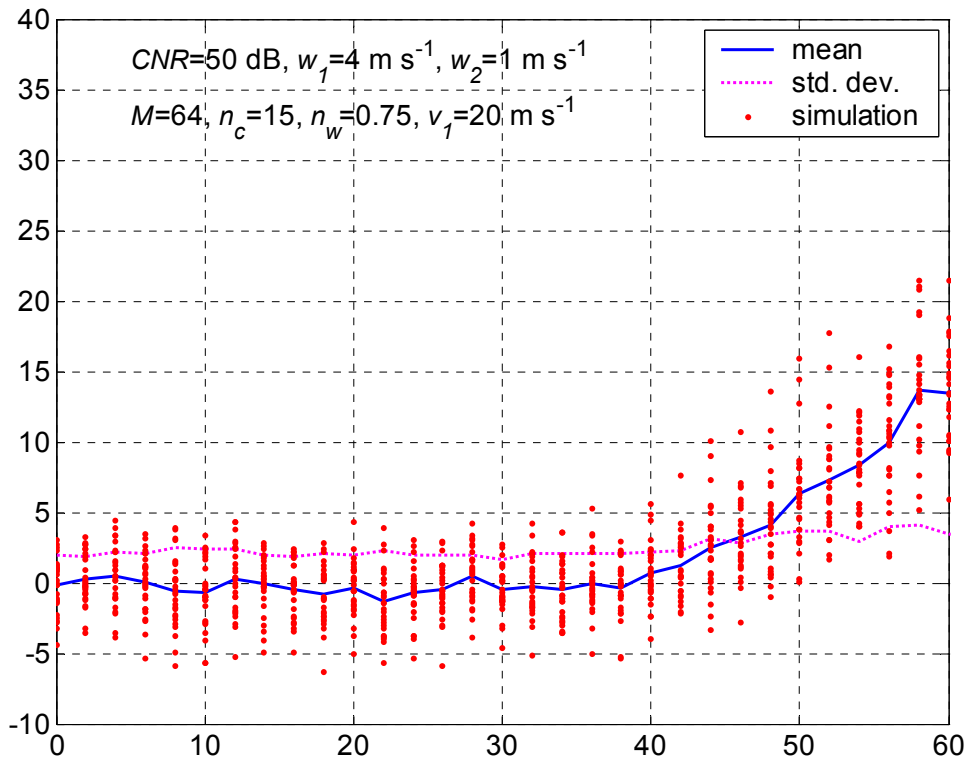


Fig. 3.11 Error in the mean power estimate, p_1 , after ground clutter filtering for $p_2/p_1 > 0$ dB for a $CSR = 50$ dB **with** the spectral restoration scheme-1, $w_2=1 \text{ m s}^{-1}$.

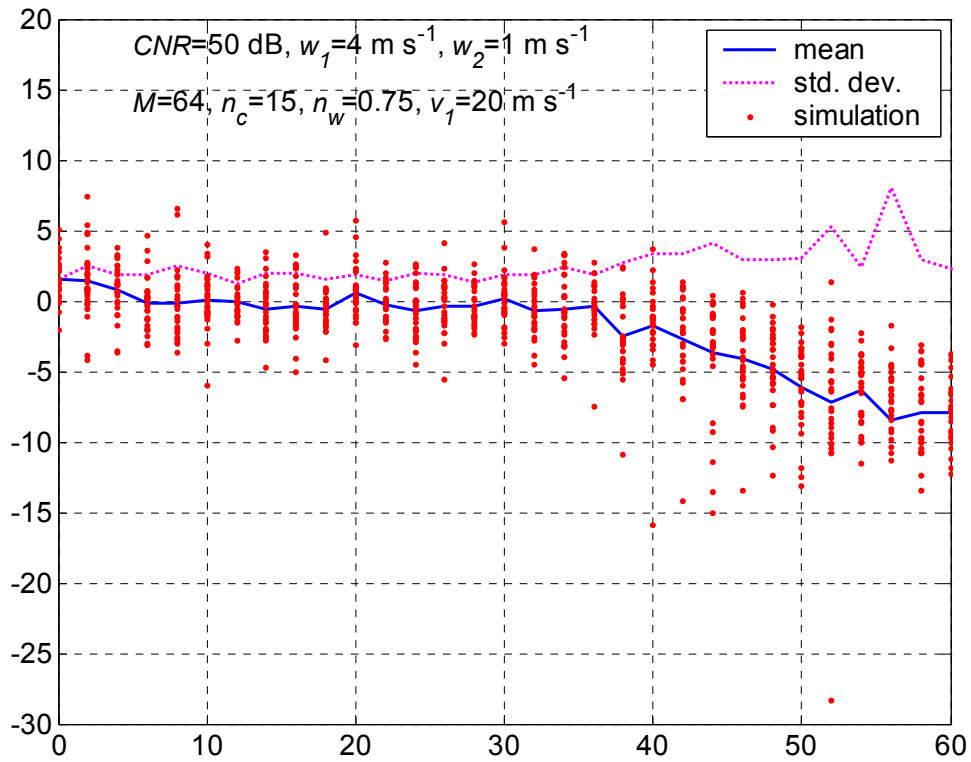


Fig. 3.12 Error in the mean velocity estimate, v_l , after ground clutter filtering for $p_2/p_1 > 0 \text{ dB}$ for a $CSR = 50 \text{ dB}$ **with** the spectral restoration scheme-1, $w_2=1 \text{ m s}^{-1}$.

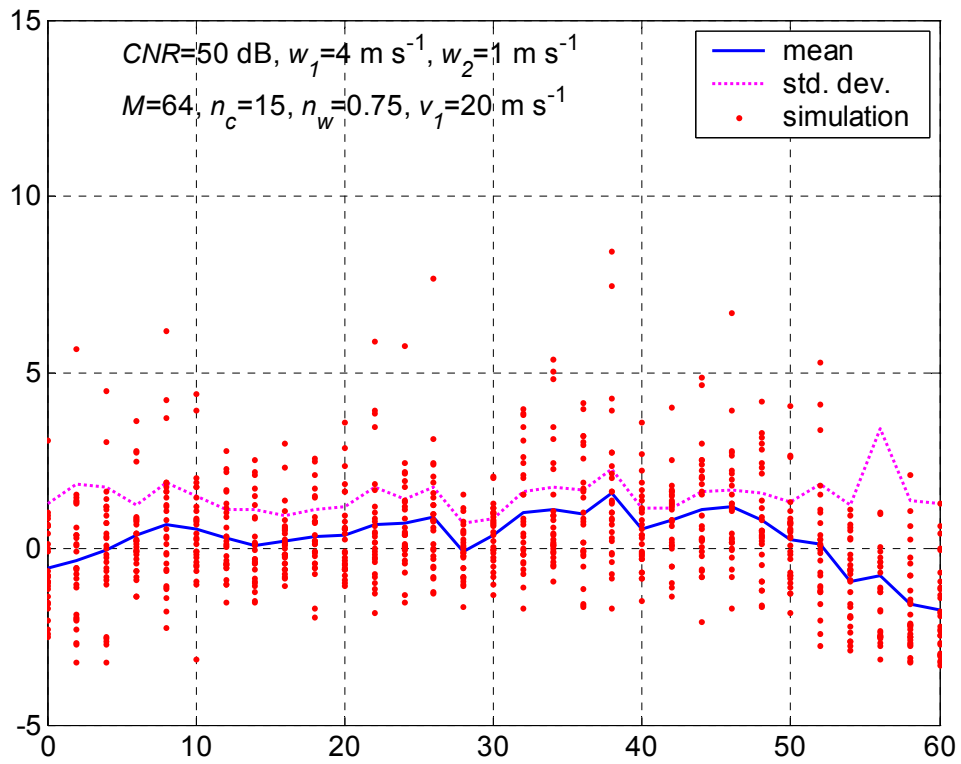


Fig.

3.13 Error in the spectrum width estimate, w_1 , after ground clutter filtering for $p_2/p_1 > 0 \text{ dB}$ for a $CSR = 50 \text{ dB}$ **with** the spectral restoration scheme-1, $w_2=1 \text{ m s}^{-1}$.

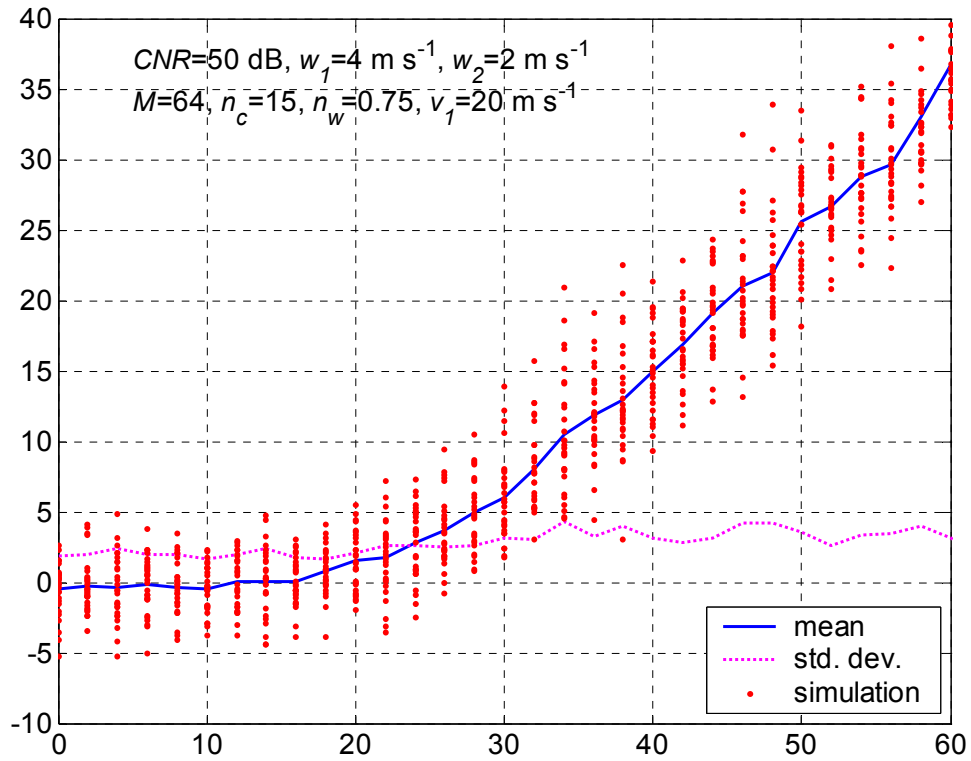


Fig. 3.14 Error in the mean power estimate, p_1 , after ground clutter filtering for $p_2/p_1 > 0$ dB for a $CSR = 50$ dB **with** the spectral restoration scheme-1, $w_2=2 \text{ m s}^{-1}$.

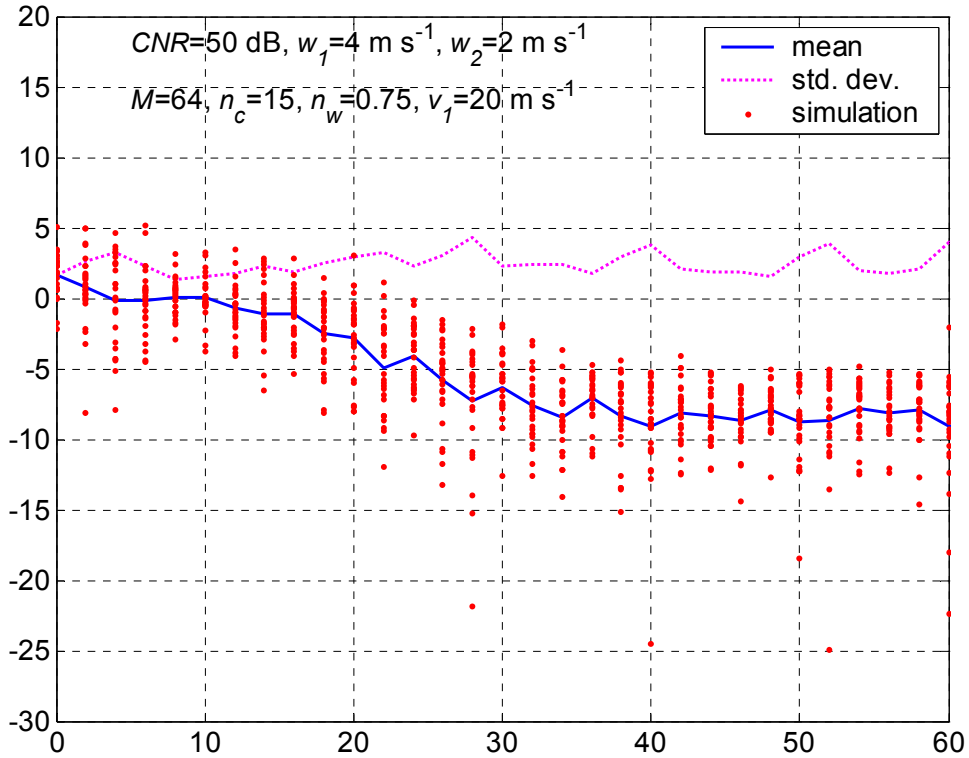


Fig. 3.15 Error in the mean velocity estimate, v_l , after ground clutter filtering for $p_2/p_1 > 0 \text{ dB}$ for a $CSR=50 \text{ dB}$ with the spectral restoration scheme-1, $w_2=2 \text{ m s}^{-1}$.

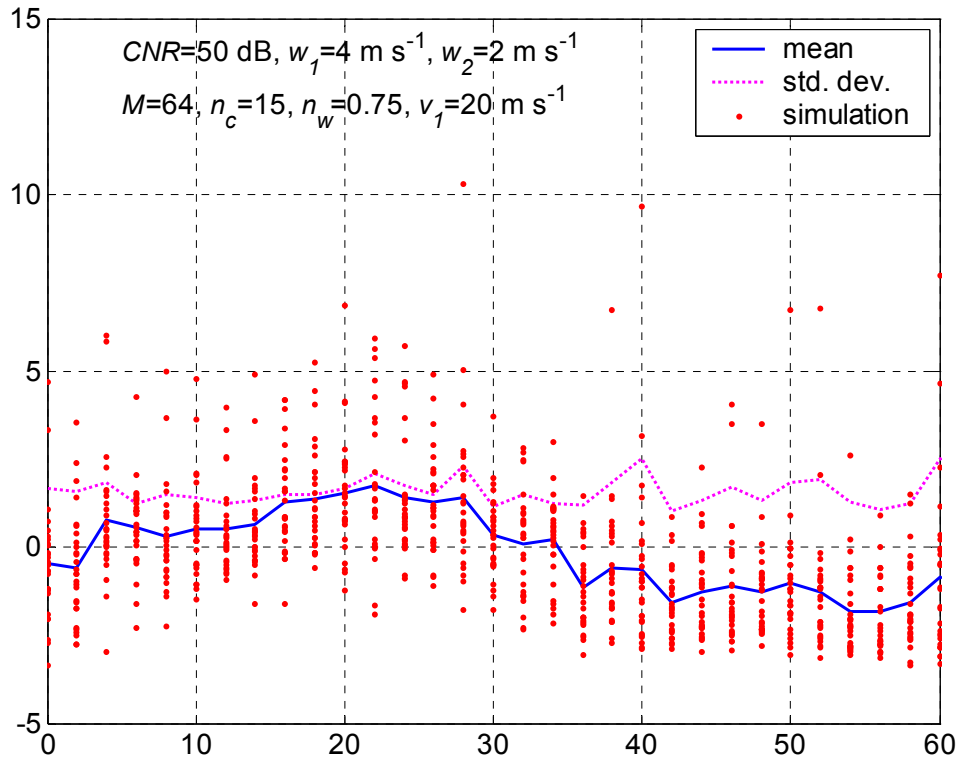


Fig. 3.16 Error in the spectrum width estimate, w_1 , after ground clutter filtering for $p_2/p_1 > 0$ dB for a $CSR = 50$ dB **with** the spectral restoration scheme-1, $w_2=2 \text{ m s}^{-1}$.

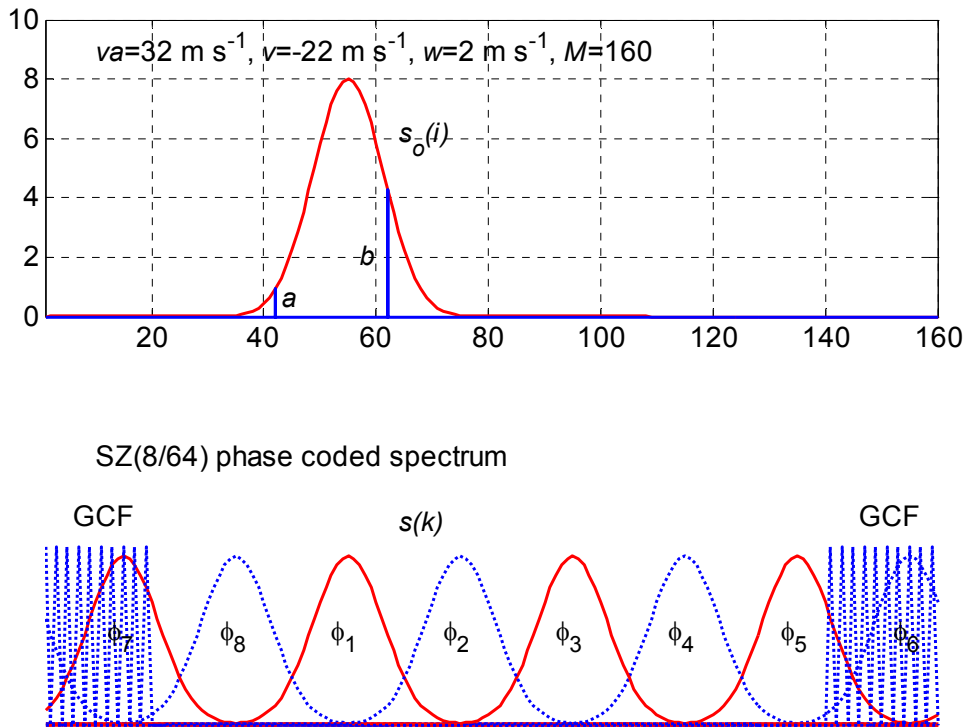


Fig. 3.17 Illustration of the SZ phase modulated spectrum and ground clutter filtering.

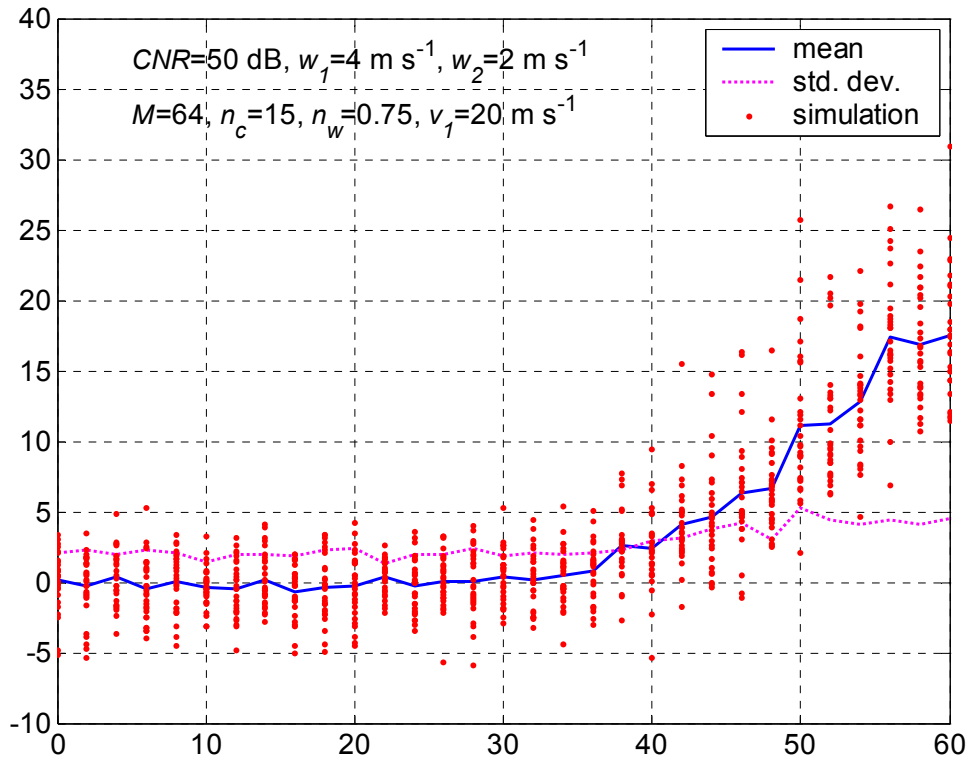


Fig. 3.18 Error in the mean power estimate, p_1 , after ground clutter filtering for $p_2/p_1 > 0$ dB for a $CSR=50$ dB **with** the spectral restoration scheme-2, $w_2=2 \text{ m s}^{-1}$.

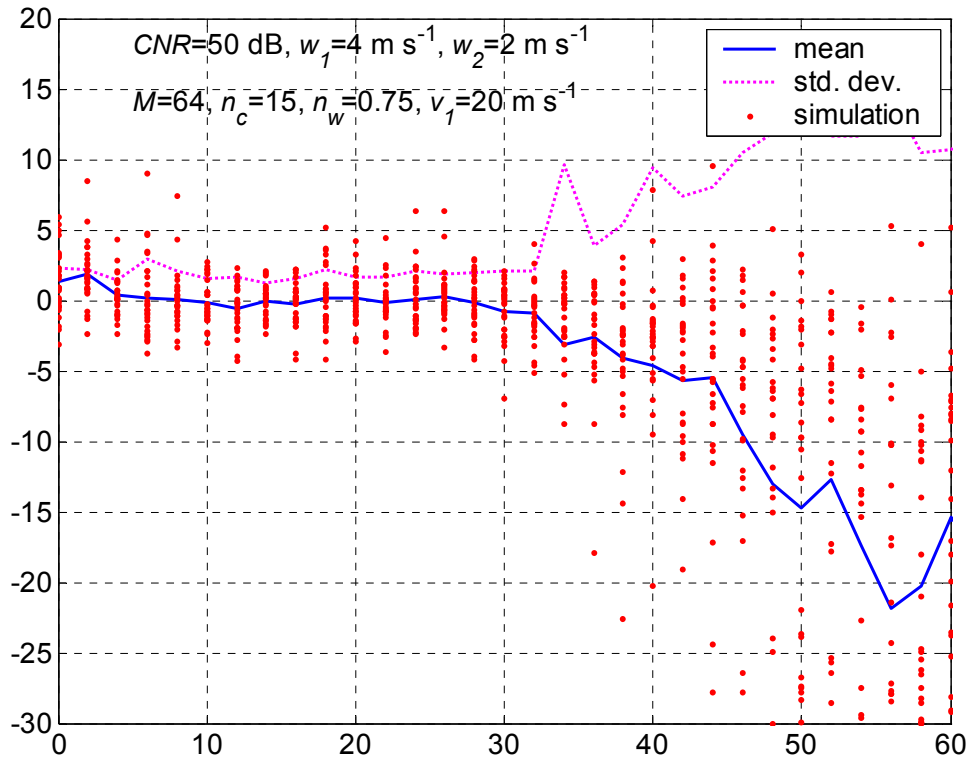


Fig. 3.19 Error in the mean velocity estimate, v_l , after ground clutter filtering for $p_2/p_1 > 0$ dB for a $CSR = 50$ dB **with** the spectral restoration scheme-2, $w_2=2 \text{ m s}^{-1}$.

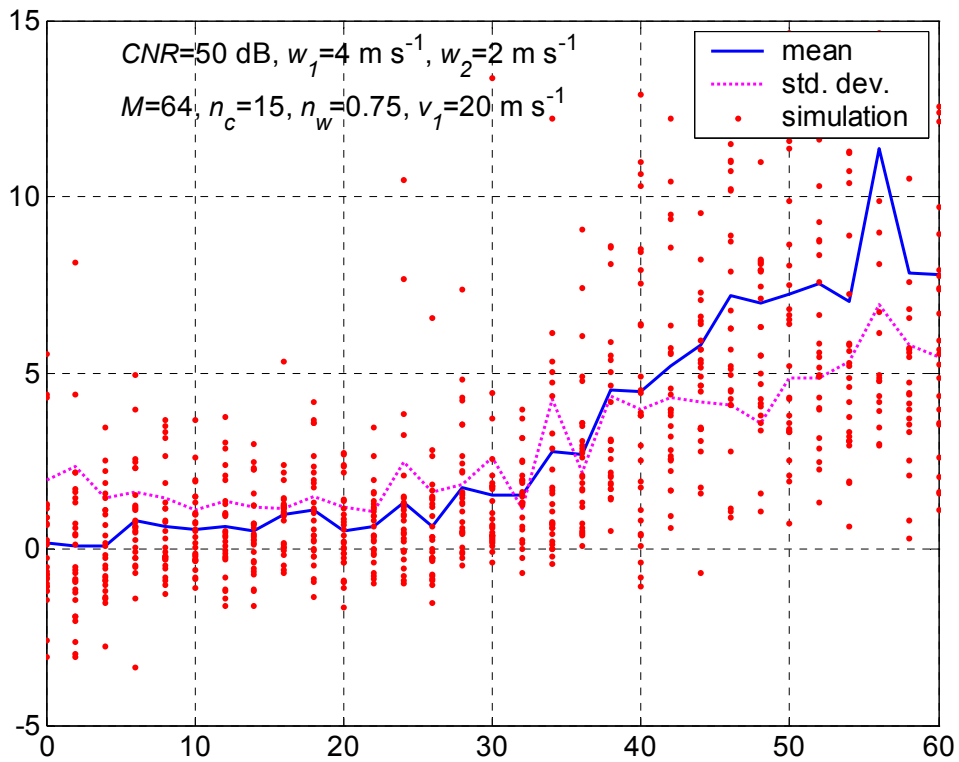


Fig. 3.20 Error in the spectrum width estimate, w_1 , after ground clutter filtering for $p_2/p_1 > 0$ dB for a $CSR = 50$ dB **with** the spectral restoration scheme-2, $w_2=2$ m s $^{-1}$.

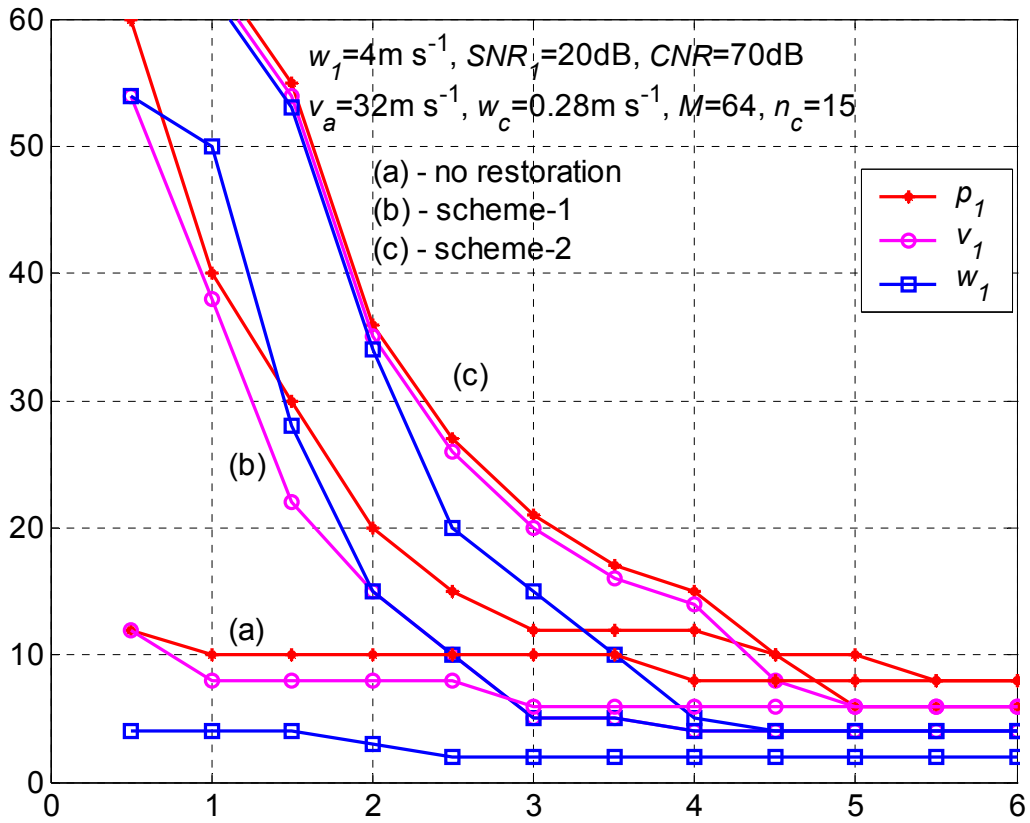


Fig. 3.21 A comparison of the performance of the spectral restoration schemes, 1 and 2, in recovering the spectral moments of the weaker 1st trip echo. The maximum p_2/p_1 ratio for which the spectral moments are recoverable is shown against the spectrum width, w_2 , of the stronger 2nd trip signal.

4. Remaining issues and further work

The fundamental recommendation for range velocity mitigation proposed in report-5 still stands. It is a hybrid scheme whereby at the two lowest elevations two consecutive scans, one at a short PRT the other at a long PRT are used. The SZ-1 algorithm should be applied to the short PRT sequence. To determine the presence of ground clutter and overlay of more than two trip echoes the long PRT is essential. It is also needed to provide the same capability as exists on the current WSR-88D network, which is unimpeded observation of reflectivity to a range of over 450 km. The main reason for phase coding at the lowest elevations is the stringent requirement for canceling ground clutter; it requires a uniform PRT. At the higher elevations the staggered PRT is the choice because it increases both the unambiguous range and velocity. Clutter strength and extent are less at higher elevations and schemes reported by Sachidananda et al. (1999, and 2000) deal effectively with it.

Thus far only one set of phase coded data from a squall line in Oklahoma is available and a couple of data sets from isolated showers in Florida have been collected. At the onset of FY-02 our plan was to collect additional phase coded data in Oklahoma. Two ways to achieve this goal have been pursued.

One, we intended to use the Sigmet processor and observe the results of their phase coding algorithm while collecting spectral moment and time series data. For that reason we have invested much time in developing software interfaces to process in real time spectral moments from Sigmet and also record these on standard workstations. ROC has enabled generation of the SZ phase code via the Sigmet processor and some data might soon become available. Nonetheless, recording of such data is limited in space and time because it requires use of an archaic recorder.

Two, the new Research RDA (RRDA) developed at NSSL has the capability to record hours of time series data and has been programmed (at the end of FY-02) to control the phase shifters. Thus it is now possible to obtain phase coded time series data without the limitations imposed by the archaic recorder.

We have abandoned our plan to observe, manipulate, and censor spectral moments produced by the Sigmet RVP7 processor with their version of the SZ phase code. The implementation on the RVP7 differs considerably from the recommended SZ-1 algorithm. Consequently recovery of the weaker signal, estimation of spectrum width, and ground clutter filtering are compromised (as explained in this report). The algorithm used by Sigmet is a clever and expedient adaptation of the

procedure that they use on random phase coded sequences. To implement the proposed SZ-1 scheme requires a fresh start and substantial development and testing by Sigmet; at present time this is unlikely in view of their commitment to develop the production RDA.

In the near term there are several things that should be done to bring the proposed mitigation scheme closer to operations. First, collect phase encoded time series data and time series of staggered PRT data. Both of these can be done on the RRDA. Application of the proposed algorithm on these data and analysis of results will provide quantitative measures of the benefits and guide us in developing effective censoring schemes. A minor variant in the SZ-1 algorithm (explained in section 3.3) on how to decide which of the echoes to process first should be spot tested. Second, implementation in steps of increased complexity should begin. Thus, we suggest implementing the simplest version of the SZ-1 phase coding and of the staggered PRT schemes. For phase coding consider only the first two trip echoes, censor higher trip echoes, and do not filter ground clutter. For staggered PRT, program the processing without clutter filter, but include censoring of one trip overlaid echo.

Issues that remain concerning the mitigation scheme are mainly in the domain of censoring and quantitative determination of effectiveness. Further, there is the question whether to extend phase coding to higher than the two lowest elevations. Other details in the phase coding scheme that must be incorporated in practice but have not been tested include a) presence of contiguous adjacent trip echoes both of which are from higher than the first trip; b) overlay in case of non contiguous echoes (like first and third trip, second and forth, first and forth); c) presence of more than two overlaid echoes; d) processing if ground clutter is part of these cases (a, b, or c). For real time application these cases must be dealt with. We suggest that in first versions of the implementation these cases be identified and censored from further processing. With experience and feedback from meteorologists it should be possible to determine which of the situations requires resolution most.

References:

1. Frush, Charles L., **1999**: NEXRAD Range-Velocity: Exploring selected mitigation techniques, 2nd year report, NCAR.
2. Cornelius, R., R. Gagnon, and F. Pratte, **1995**: WSR-88D Clutter processing and AP clutter mitigation., *Interagency MOU between OSF and FSL, Final report submitted by FSL-ATD engineering team*. 182 pages.
3. Doviak, R. J. and D.S. Zrnice, **1993**: 'Doppler radar and weather observations.' Academic Press, New York, 562p.
4. Frush, C. L., R. J. Doviak, M. Sachidananda, and D.S. Zrnice, **2002**: Application of the SZ phase code to mitigate range-velocity ambiguities in weather radars. *Journal of Atmospheric and Oceanic Technology*, vol.19, No.4, pp 413-430.
5. Sachidananda, M., D. S. Zrnice, and R. J. Doviak, **1998**: Signal design and processing techniques for WSR-88D ambiguity resolution, Part-2. *National Severe Storms Laboratory*, June 1998, 105 pp.
6. Siggia, A, and R. Passarelli, **2002**, SZ(8/64) and other phase codes, SIGMET internal notes, April 2002.
7. Sirmans, D., **1992**: Clutter filtering in the WSR-88D, NWS/OSF, Norman, OK.
8. Ming Fang and R.J. Doviak, 2001: Spectrum width statistics of various weather phenomena. *National Severe Storms Laboratory*, September 2001, 62 pp.

**LIST OF NSSL REPORTS FOCUSED ON
POSSIBLE UPGRADES TO THE WSR-88D RADARS.**

1. Sachidananda, M., **2001**: Signal Design and Processing Techniques for WSR-88D Ambiguity Resolution, Part V, 75 pp.
2. Sachidananda, M., **2000**: Signal Design and Processing Techniques for WSR-88D Ambiguity Resolution, Part IV, 99 pp.
3. Sachidananda, M., **1999**: Signal Design and Processing Techniques for WSR-88D Ambiguity Resolution, Part III, 81 pp.
4. Doviak, R. J. and D. S. Zrnic, **1998**: NOAA/NSSL's WSR-88D Radar for Research and Enhancement of Operations: Polarimetric Upgrades to Improve Rainfall Measurements, 110 pp.
5. Sachidananda, M., **1998**: Signal Design and Processing Techniques for WSR-88D Ambiguity Resolution, Part II, 105 pp.
6. Sachidananda, M., **1997**: Signal Design and Processing Techniques for WSR-88D Ambiguity Resolution, Part I, 100 pp.
7. Sirmans, D., D. S. Zrnic, and M. Sachidananda, **1986**: Doppler radar dual polarization considerations for NEXRAD, Part I, 109 pp.
8. Sirmans, D., D. S. Zrnic, and N. Balakrishnan, **1986**: Doppler radar dual polarization considerations for NEXRAD, Part II, 70 pp.